

Magnetic properties of $\text{CoBr}_{2.6}[(1-x)\text{H}_2\text{O}-x\text{D}_2\text{O}]$

Citation for published version (APA):

Hijmans, J. P. A. M. (1979). *Magnetic properties of $\text{CoBr}_{2.6}[(1-x)\text{H}_2\text{O}-x\text{D}_2\text{O}]$* . [Phd Thesis 1 (Research TU/e / Graduation TU/e), Applied Physics and Science Education]. Technische Hogeschool Eindhoven.
<https://doi.org/10.6100/IR90899>

DOI:

[10.6100/IR90899](https://doi.org/10.6100/IR90899)

Document status and date:

Published: 01/01/1979

Document Version:

Publisher's PDF, also known as Version of Record (includes final page, issue and volume numbers)

Please check the document version of this publication:

- A submitted manuscript is the version of the article upon submission and before peer-review. There can be important differences between the submitted version and the official published version of record. People interested in the research are advised to contact the author for the final version of the publication, or visit the DOI to the publisher's website.
- The final author version and the galley proof are versions of the publication after peer review.
- The final published version features the final layout of the paper including the volume, issue and page numbers.

[Link to publication](#)

General rights

Copyright and moral rights for the publications made accessible in the public portal are retained by the authors and/or other copyright owners and it is a condition of accessing publications that users recognise and abide by the legal requirements associated with these rights.

- Users may download and print one copy of any publication from the public portal for the purpose of private study or research.
- You may not further distribute the material or use it for any profit-making activity or commercial gain
- You may freely distribute the URL identifying the publication in the public portal.

If the publication is distributed under the terms of Article 25fa of the Dutch Copyright Act, indicated by the "Taverne" license above, please follow below link for the End User Agreement:

www.tue.nl/taverne

Take down policy

If you believe that this document breaches copyright please contact us at:

openaccess@tue.nl

providing details and we will investigate your claim.

MAGNETIC PROPERTIES OF $\text{CoBr}_2 \cdot 6[(1-x)\text{H}_2\text{O} \cdot x\text{D}_2\text{O}]$

J.P.A.M. Hijmans

MAGNETIC PROPERTIES OF $\text{CoBr}_2 \cdot 6[(1-x)\text{H}_2\text{O} \cdot x\text{D}_2\text{O}]$

PROEFSCHRIFT

TER VERKRIJGING VAN DE GRAAD VAN DOCTOR IN DE
TECHNISCHE WETENSCHAPPEN AAN DE TECHNISCHE
HOOGESCHOOL EINDHOVEN, OP GEZAG VAN DE RECTOR
MAGNIFICUS, PROF. DR. P. VAN DER LEEDEN, VOOR
EEN COMMISSIE AANGEWEEZEN DOOR HET COLLEGE
VAN DEKANEN IN HET OPENBAAR TE VERDEDIGEN OP
DINSDAG 29 MEI 1979 TE 16.00 UUR

DOOR

JOANNES PETRUS ANTONIUS MARIA HIJMANS

GEBOREN TE EINDHOVEN

DIT PROEFSCHRIFT IS GOEDGEKEURD
DOOR DE PROMOTOREN

Prof.dr. P. van der Leeden

en

Prof.dr. M.J. Steenland

TABLE OF CONTENTS

I	INTRODUCTION	1
	<i>References</i>	4
II	EXPERIMENTAL METHODS	
	2.1 <i>Introduction</i>	5
	2.2 <i>Sample preparation</i>	5
	2.3 <i>Specific heat</i>	5
	2.4 <i>Antiferromagnetic resonance</i>	7
	2.5 <i>Nuclear magnetic resonance</i>	8
	2.6 <i>Static susceptibility</i>	9
	2.7 <i>Dynamic susceptibility</i>	11
	2.8 <i>References</i>	12
III	HIGH-TEMPERATURE SUSCEPTIBILITY	
	3.1 <i>Introduction</i>	13
	3.2 <i>Theory</i>	15
	3.3 <i>Experimental results</i>	21
	3.4 <i>Discussion</i>	28
	3.5 <i>References</i>	31
IV	SPECIFIC HEAT	
	4.1 <i>Introduction</i>	32
	4.2 <i>Experimental results</i>	32
	4.3 <i>Exchange interactions</i>	39
	4.4 <i>References</i>	43
V	DISCUSSION ON $\text{CoBr}_2 \cdot 6\text{H}_2\text{O}$	
	5.1 <i>Introduction</i>	44
	5.2 <i>Molecular Field approximations</i>	44
	5.3 <i>Spatial dimensionality</i>	50
	5.4 <i>References</i>	53

VI	ISOTOPE EFFECTS	
	6.1 Introduction	54
	6.2 Experimental results	
	<i>Antiferromagnetic resonance</i>	54
	<i>The critical field</i>	56
	<i>Proton resonance</i>	56
	<i>Bromine nuclear resonance</i>	58
	6.3 Discussion	64
	6.4 References	71
	SAMENVATTING	72
	DANKWOORD	74
	LEVENSBERICHT	75

CHAPTER I

INTRODUCTION.

The qualitatively similar magnetic behaviour of $\text{CoBr}_2 \cdot 6\text{H}_2\text{O}$ and $\text{CoCl}_2 \cdot 6\text{H}_2\text{O}$ has been the subject of a considerable number of both experimental and theoretical studies. These studies include specific heat measurements¹⁾, nuclear magnetic resonance^{2,3)} antiferromagnetic resonance^{4,5)}, susceptibility measurements⁶⁾, optical absorption experiments⁷⁾ and calculation of the Co^{2+} ground state⁸⁾. References 2 and 5 refer to the bromide, references 1, 4, 6 and 8 to the chloride and references 3 and 7 to both substances.

Initially, most of the attention was directed to the chlorine compound and research on $\text{CoBr}_2 \cdot 6\text{H}_2\text{O}$ was mainly performed in order to investigate the effects of Cl-Br substitution. When the idea that these compounds might be two of the very rare fairly good approximations of the two-dimensional XY model started to settle, it became desirable to detect the, presumably small, deviations from the ideal model. The investigations described in this thesis were intended as a contribution to the research in this direction. Moreover, it became clear in the earlier stages of these investigations that the crystallographic structures of $\text{CoCl}_2 \cdot 6\text{H}_2\text{O}$ and $\text{CoBr}_2 \cdot 6\text{H}_2\text{O}$ are close to their limit of stability. At percentages of deuteration of 3.5% and 55%, respectively, a change in crystallographic structure, accompanied by a rather curious magnetic behaviour at lower temperatures, is observed. It does not seem unlikely that these effects are somehow related to the recently claimed observation of an intermediate state in the magnetic phase diagram of the bromide⁹⁾. So, we thought it worthwhile to study the anomalous effects upon deuteration rather in detail. In spite of the fact that the properties of $\text{CoCl}_2 \cdot 6\text{H}_2\text{O}$ were better documented we concentrated on the bromide, mainly because this compound is better suited for neutron diffraction experiments, which were planned in connection with this work.

To get an impression of the extent, to which the interactions in $\text{CoBr}_2 \cdot 6\text{H}_2\text{O}$ might be approximated by a two-dimensional XY model, we turn to the crystallographic structure^{10,11,12)} of this salt. The structure can be described by the monoclinic face-centered spacegroup C_{2h}^2 and a unit-cell, with $a = 11.03 \text{ \AA}$, $b = 7.16 \text{ \AA}$, $c = 6.91 \text{ \AA}$ and $\beta = 124^\circ$,

containing two formula units. The spatial arrangement of the CoBr_2O_4 clusters is shown in fig. I-1a while some details of the cluster itself are given in fig. I-1b. The clusters are all equivalent and the Br-Co-Br axis is almost perpendicular (88.7°) to the plane of the oxygen atoms, which are situated at the corners of a rectangle with almost equal sides.

In general, both exchange and dipolar interactions will contribute to the coupling between Co^{2+} ions. However, the dipolar contribution may often be neglected in nearest neighbour interactions since it is generally very small compared to the exchange interaction. The nearest neighbour interaction between Co atoms in the face centered ab plane (denoted by J_1 in fig. I-1a) involves exchange paths like Co-Br-Br-Co and Co-Br- H_2O -Co. The exchange contribution to the coupling J_2 between adjacent atoms in the b direction originates from links like Co-OH₂- H_2O -Co and will presumably be smaller⁶⁾, in view of the relative weakness of hydrogen bonds. Because of the large interatomic distance along the a axis (11.0 \AA), the interaction J_3 must be considered as negli-

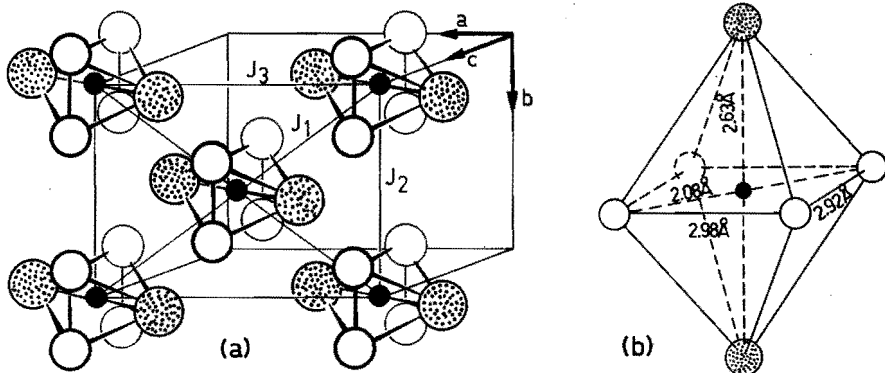


Figure I-1.

Details of the crystallographic structure of $\text{CoBr}_2 \cdot 6\text{H}_2\text{O}$. Cobalt atoms are small and black, bromine atoms are shaded and oxygen atoms are drawn as open circles.

- (a) The face-centered arrangement of the CoBr_2O_4 clusters in the ab plane. J_1 , J_2 and J_3 denote the exchange interactions discussed in the text.
- (b) Some distances within the CoBr_2O_4 cluster. The smallest distance between two oxygen atoms is found in the b direction.

bly small. The coupling between the ab layers probably consists of exchange paths involving water molecules not belonging to the $\text{CoBr}_2 \cdot 6\text{H}_2\text{O}$ clusters and is therefore expected to be very weak^{6,13}). This conjecture is supported by the perfect cleavage of the crystals along the ab plane. So, it seems that the spatial distribution of the interactions can reasonably well be approximated by a two-dimensional model, only involving J_1 and J_2 , if dipolar interactions are of minor importance.

The approximately fourfold symmetry around the Br-Co-Br axis of the clusters, in combination with the strong uniaxial effect caused by the two bromine atoms, suggests that, at low temperatures, the magnetic moment on the Co atoms will show a strong, almost uniaxial, anisotropy. It is generally accepted (see chapter III) that this anisotropy results in an analogous property of the exchange tensors $\vec{J}_{m,n}^{\pm}$, which describe the interaction between the effective spins \vec{S}_m and \vec{S}_n according to

$$H_{m,n} = -2 (J_{m,n}^x S_m^x S_n^x + J_{m,n}^y S_m^y S_n^y + J_{m,n}^z S_m^z S_n^z) . \quad (1)$$

If we choose the z axis (approximately) along the Br-Co-Br axis this means that $J_{m,n}^x \approx J_{m,n}^y$ and that either $|J_{m,n}^x| \gg |J_{m,n}^z|$ or $|J_{m,n}^x| \ll |J_{m,n}^z|$. The first of these inequalities leads to an XY-like behaviour since the two-spin Hamiltonian for an XY system is

$$H_{m,n}^{XY} = -2 J_{m,n}^{XY} (S_m^x S_n^x + S_m^y S_n^y) . \quad (2)$$

The second inequality would result in an Ising-like description, which is excluded for $\text{CoBr}_2 \cdot 6\text{H}_2\text{O}$ by experimental evidence. Comparison of eqs. 1 and 2 immediately reveals two reasons why the XY model should not hold exactly. First, symmetry does not require that $J_{m,n}^x = J_{m,n}^y$ and, secondly, there is no apparent reason for $J_{m,n}^z$ to vanish. Furthermore, it should be stressed that the arguments used to arrive at an XY-like model are only valid for $kT \ll \Delta$, where Δ is an energy connected with the Hamiltonian which represents the uniaxial anisotropy. This implies that one has to account for the influence of excited levels under certain circumstances. Curiously enough, this influence is not always restricted to higher temperatures as will be shown from the susceptibility data (chapter III).

We wish to close this introduction with a short outline of this thesis. The experimental techniques we employed will be described in

chapter II. In chapter III, the high-temperature behaviour of the susceptibility will be analyzed in terms of a crystal-field model combined with a high-temperature expansion for the exchange contribution. This analysis, made under the assumptions that $\tilde{J}_2 = \tilde{J}_0$ and $J_1^x = J_1^y$, will yield quantitative results for the g-values and the main interaction \tilde{J}_1 . Chapter IV will mainly be concerned with the high-temperature behaviour of the specific heat in order to obtain an estimate for the interaction \tilde{J}_2 . Information obtained from several kinds of experiments performed in the ordered state below T_N^x will be presented in chapter V. Here, the XY plane anisotropy $J_1^x - J_1^y$ will be deduced from antiferromagnetic resonance data and attention will be paid to the spatial dimensionality of the system. Besides, a comparison of parameters determined from experiments below and above T_N will be made. Finally, the effects of deuteration will be discussed in chapter VI.

References.

- 1) W.K. Robinson and S.A. Friedberg, Phys. Rev. 117, 402 (1960).
- 2) K.V.S. Rama Rao, W.J.M. de Jonge and C.H.W. Swüste, Physica 53, 621 (1971).
- 3) R.D. Spence, P. Middents, Z.El Saffar and R. Kleinberg, J. Appl. Phys. 35, 854 (1964).
- 4) M. Date, J. Phys. Soc. Japan 16, 1337 (1961).
- 5) T.E. Murray and G.K. Wessel, J. Phys. Soc. Japan 24, 738 (1968).
- 6) T. Haseda, J. Phys. Soc. Japan 15, 483 (1960).
- 7) R. Pappalardo, Phil. Mag. 4, 219 (1959).
- 8) N. Uryu, J. Skalyo and S.A. Friedberg, Phys. Rev. 144, 689 (1966).
- 9) J.A.J. Basten, Ph.D. Thesis, Eindhoven (1979).
- 10) J. Mizuno, J. Phys. Soc. Japan 15, 1412 (1960).
- 11) E.V. Stroganov, S. Andreev, Kochina and V. Soloviev, Vestn. Leningrad. Univ. Ser. Fiz. Khim. 16, 114 (1961).
For a comment on this structure determination see ref. 5.
- 12) J.A.J. Basten and A.L.M. Bongaarts, Phys. Rev. B14, 2119 (1976).
- 13) R. Kleinberg, J. Chem. Phys. 53, 2660 (1970).

CHAPTER II

EXPERIMENTAL METHODS.

2.1 *Introduction.*

In this chapter we will briefly consider the preparation of $\text{CoBr}_2 \cdot 6[(1-x)\text{H}_2\text{O} \cdot x\text{D}_2\text{O}]$ samples and the experimental techniques we used to study these compounds. With the exception of specific heat measurements, all other experiments, i.e. static and dynamic susceptibility measurements, nuclear magnetic resonance and antiferromagnetic resonance, require oriented single crystals. These crystals were always oriented using an X-ray diffractometer.

2.2 *Sample preparation.*

Crystals of $\text{CoBr}_2 \cdot 6\text{H}_2\text{O}$ were grown by evaporation of a saturated aqueous solution at room temperature. Partially deuterated samples were prepared by evaporation of a solution of anhydrous CoBr_2 in a mixture of normal and heavy water under a stream of dry nitrogen gas. The anhydrous CoBr_2 was obtained by slowly heating the hydrate up to 90°C in vacuo. It was inferred from neutron diffraction experiments that the percentage of deuterium in the samples of $\text{CoBr}_2 \cdot 6[(1-x)\text{H}_2\text{O} \cdot x\text{D}_2\text{O}]$ corresponds rather well to the ratio of normal and heavy water in the solutions. A solution containing 50% D_2O yielded crystals with $x = 0.48 \pm 0.02$ ¹⁾ while a 100% D_2O solution resulted in $x = 0.93 \pm 0.02$ ²⁾. These differences, which are probably due to incomplete dehydration of the hydrate upon heating in vacuo, are of little practical consequence in the present context and will therefore be neglected.

2.3 *Specific heat.*

Specific heat measurements were performed with an adiabatic calorimeter which is schematically shown in figure II-1. The samples, consisting of ≈ 0.1 mole of crystals with an average linear dimension of 5 mm, were sealed in a copper capsule together with a little ^3He gas (< 10 mm Hg at 77 K) to speed up the rate at which thermal equilibrium is reached. Heat inputs were supplied through a manganese heater which was bifilar-

ly wound around the capsule. Both current and voltage were measured during a heating period. Temperatures were determined with a calibrated germanium resistor having a nominal resistance of $1 \text{ k}\Omega$ at 4.2 K . This thermometer was incorporated in a 170 Hz Wheatstone bridge employing a 10 mV driving voltage to avoid excessive self-heating and a lock-in amplifier as the null detector. A discontinuous heating technique was used, i.e. the temperature increase of the sample plus sample holder upon an accurately known heat input was measured. The heat capacity of the capsule was measured in a separate run. Its contribution to the total heat capacity amounted to about 0.5% at 1.2 K and 30% at 11 K . The overall accuracy of the specific heat measurements is estimated to be better than 1% .

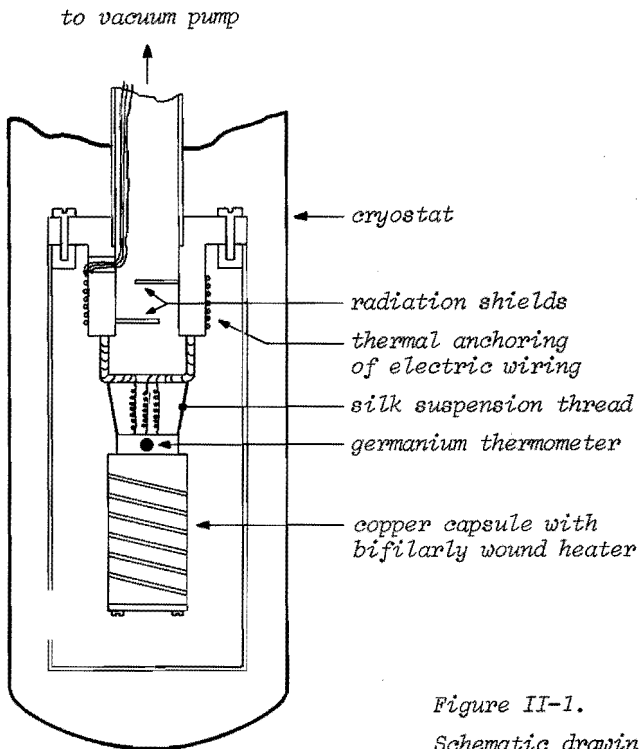


Figure II-1.
Schematic drawing of the
adiabatic calorimeter.

2.4 Antiferromagnetic resonance (AFMR).

Because AFMR signals generally are strong, we could use the simple type of spectrometer sketched in figure II-2 to detect the resonances. Microwave radiation generated by a klystron first passes an attenuator, a frequency meter and again an attenuator to prevent frequency pulling on the klystron and on the frequency meter. In this way the power level is

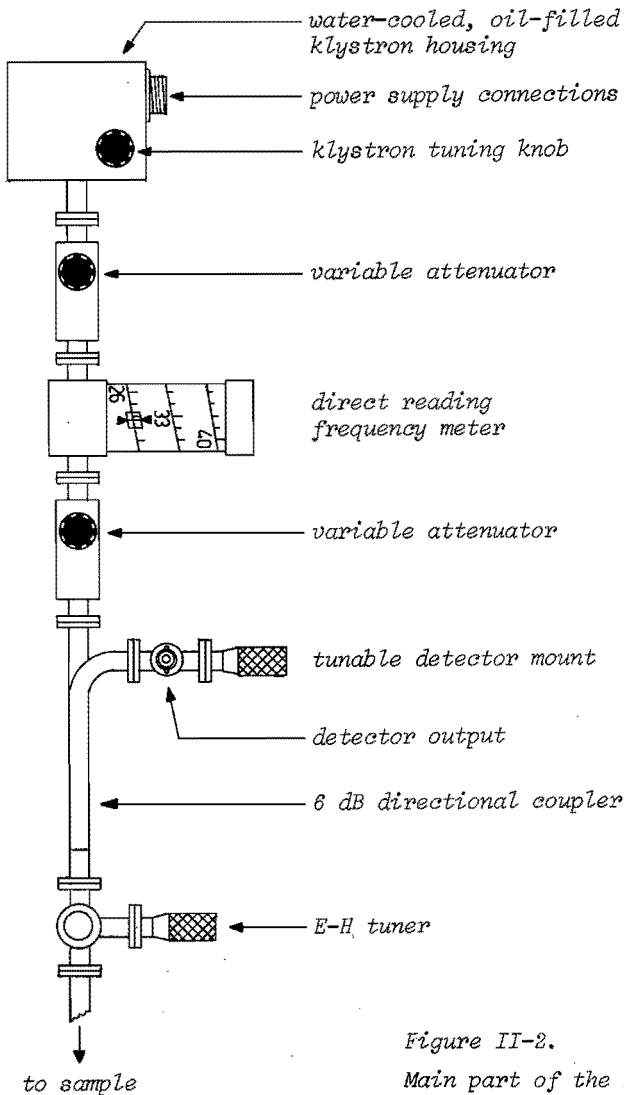


Figure II-2.
Main part of the microwave circuit of the AFMR-spectrometer.

reduced from typically 100 mW to 1 mW. With the aid of a tuner, which acts as a variable transformer, and a directional coupler most of the remaining power is reflected directly to the detector diode in order to bias the diode. This bias is needed to obtain a compromise between gain and noise of the detector. The rest of the power passes through a pressure window and a piece of stainless steel wave-guide before reaching the sample immersed in liquid ^4He . The sample is glued to the narrow wall of the wave-guide at approximately (sample dimensions are usually not small compared to the wave-length) a quarter of a wave-length from the shortcircuited end of the wave-guide. The power, reflected by the sample at resonance, is varied at a frequency of 270 Hz by modulation coils on the poles of a conventional magnet supplying the static field, converted into a voltage by the detector diode and fed to a lock-in amplifier operating at the modulation frequency. Finally the d.c. output of the lock-in amplifier is displayed on an XY-recorder whose horizontal axis is driven proportional to the magnetic field strength.

So far, we did not mention a significant experimental complication which arises in measuring a complete frequency-field diagram (see chapters V, VI). Most microwave components, such as for instance a simple attenuator, can only work properly in a rather restricted frequency range because their design is based upon the existence of a single mode in the wave-guide and the specific properties of wave-propagation in that mode. To give an impression, the region from 8 to 90 GHz is divided into "bands" as follows: 8-12 GHz, 12-18 GHz, 18-26 GHz, 26-40 GHz, 40-60 GHz and 60-90 GHz. So, generally one needs several experimental set-ups as sketched in figure II-2 to obtain a reasonably good picture of an AFMR diagram.

2.5 Nuclear magnetic resonance (NMR).

The NMR data were collected with a modified Pound-Watkins marginal oscillator³⁾ and second harmonic detection. Oscillator coils were wound directly on the crystals thus obtaining a maximum filling factor. To improve the quality of the resonance circuit for frequencies above 20 MHz, a short (approximately 60 cm in length) cryostat was used and the length of coaxial cable outside the cryostat was kept as short as possible. The modulation field, with a frequency of 135 Hz, was provided by a pair of Helmholtz coils outside the cryostat (see figure

II-3) and could be rotated around a vertical axis. Samples were mounted on a goniometer which allowed 360° rotation around a horizontal axis. The position of this axis with respect to the modulation field could be found from the voltage induced by the modulation field in a flat pick-up coil mounted on the goniometer. Temperatures were determined by measuring the vapour pressure above the ^4He bath in which the sample was immersed.

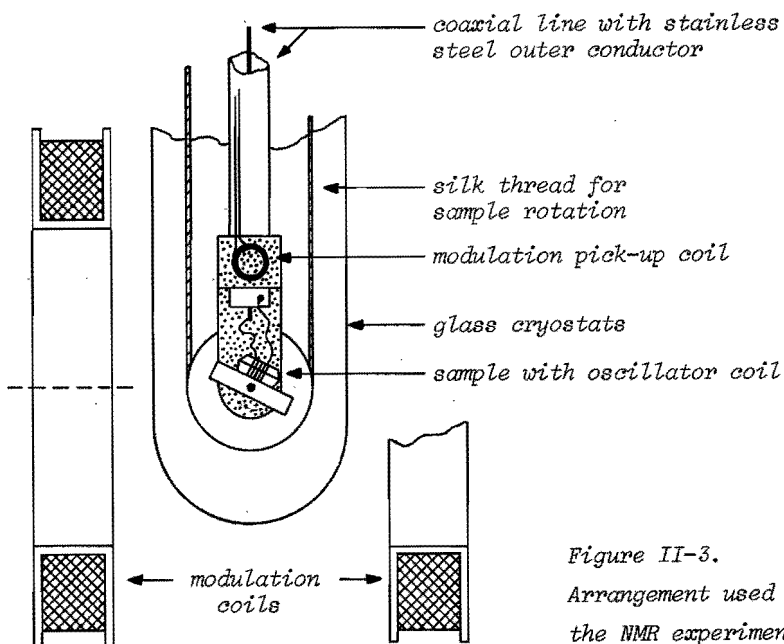


Figure II-3.
Arrangement used in
the NMR experiments.

2.6 Static susceptibility.

Static magnetization and susceptibility measurements were performed with a Faraday balance. A schematic drawing of this instrument is given in figure II-4. The sample is placed in an inhomogeneous field region slightly above the poles of a conventional magnet. With the field in the x direction, a sufficiently small sample will experience a force of which the component in the (vertical) z direction is directly propor-

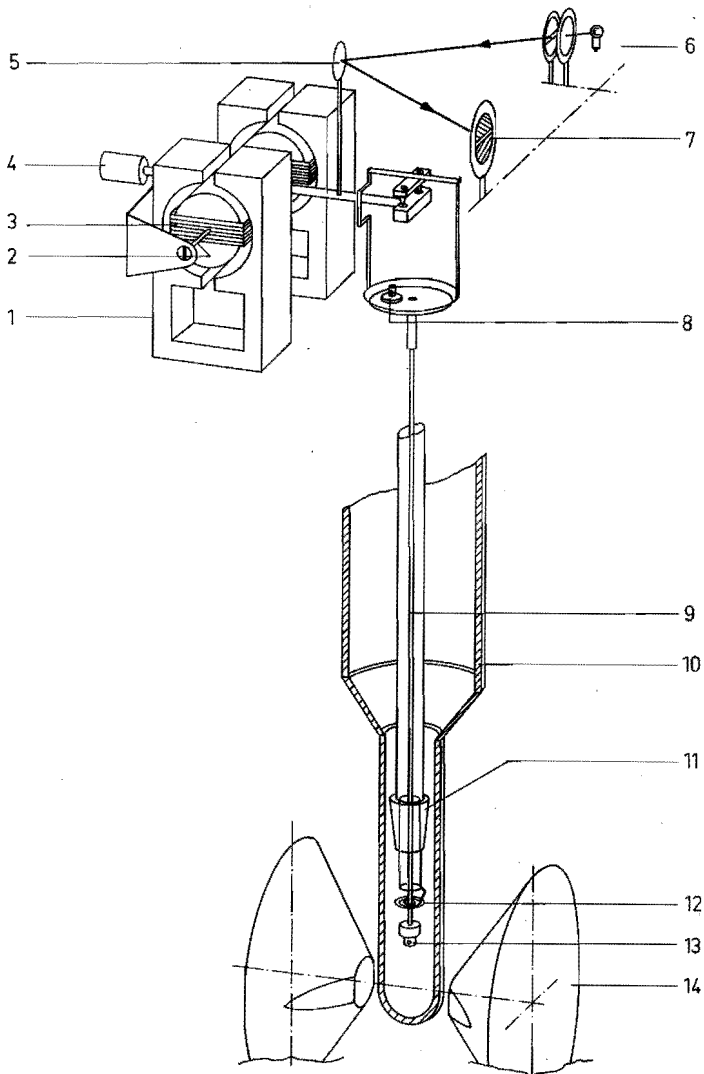


Figure II-4.

Schematic picture of the Faraday balance.

1 - permanent magnet; 2 - torsion strip; 3 - compensation coil;
 4 - counter weight; 5 - mirror; 6 - light source; 7 - differential
 photovoltaic cell; 8 - calibration weight; 9 - quartz rod;
 10 - cryostat; 11 - conical joint to which a glass protection tube can
 be attached in order to eliminate disturbances caused by boiling of the
 cooling liquids; 12 - flat coiled spring to keep the quartz rod (9)
 centered; 13 - sample holder; 14 - magnet poles.

tional to $\sigma_x \partial H_x / \partial z$, where σ_x is the x-component of the resulting magnetization. This component of the force is transferred to a balance on top of the cryostat by means of a long rod to which the sample is attached. The current through the compensation coils of the balance is adjusted by an optical feed back system in order to maintain equilibrium and is thus a measure for the magnetization σ_x of the sample. Susceptibilities are inferred from the slope of the magnetization curve. With the design described here, and in more detail in references 4 and 5, it was only possible to measure in the temperature ranges provided by the usual cooling liquids such as ^4He , H_2 and N_2 .

2.7 Dynamic susceptibility.

The dynamic susceptibility data were mainly collected because they could be obtained in a wider temperature region than the static measurements. Although, on itself, they do not give absolute values, combination with the static absolute values gives reliable results over a rather wide temperature range.

In the experimental set-up a mutual inductance bridge method was used^{5,6}). The apparatus consists essentially of a coil system wound in such a way that the mutual inductance between primary and secondary should be zero in the absence of a sample⁵). The current through the primary coil is sinusoidal with a frequency of 1000 Hz. The dynamic response of the sample, $\chi_{\text{dyn}} = \chi' - i\chi''$, leads to a voltage across the secondary coil of which both the in-phase and out-of-phase component with respect to the primary voltage can be measured by means of a compensation network. If the frequency of the bridge voltage is low compared to the lowest relaxation rate that plays a role in the sample, χ'' is zero within experimental accuracy and χ' may be equated to the static susceptibility. In order to correct for the non-ideal behaviour of the empty coil system, the sample and its holder can be moved in and out of the coils during the actual measurements. The effect of the empty sample holder has to be measured in a separate run.

Temperatures were established as follows (see figure II-5). A vacuum tight can, in which the coil system is mounted, is immersed in the cooling liquid inside a cryostat. Between this can and the coils a heat shield is situated of which the temperature can be raised using a bifilarly wound heater. To ensure temperature homogeneity the can is

filled with a little ^4He contact gas. (Normally a pressure of about 1 mm Hg was used). The temperature is measured with a calibrated germanium thermometer mounted close to the coils inside the heat shield.

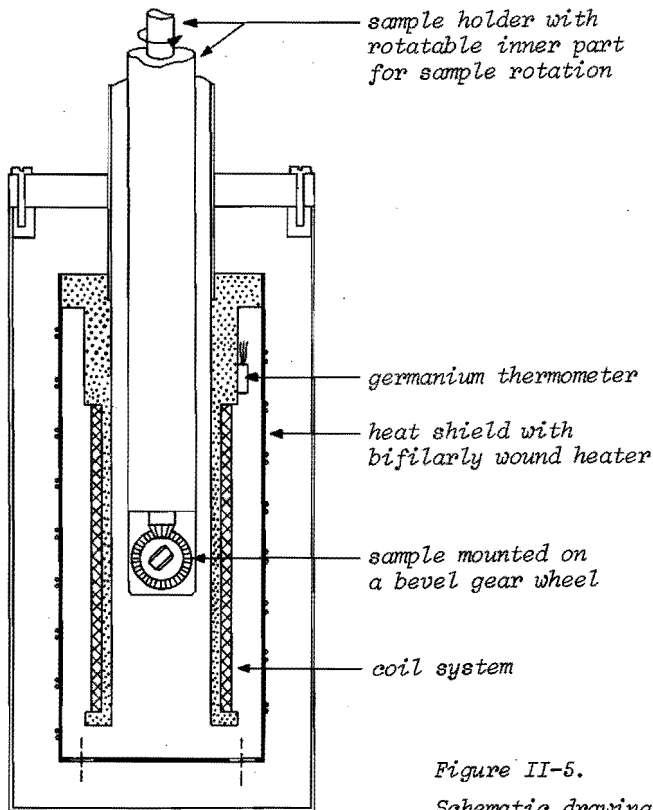


Figure II-5.
Schematic drawing of the insert intended for dynamic susceptibility measurements.

2.8 References.

- 1) J.A.J. Basten, Proc. of the Int. Symp. on Neutron Inelastic Scattering (IAEA, Vienna 1978), Vol. II, 247.
- 2) J.A.J. Basten and A.L.M. Bongaarts, Phys. Rev. B 14, 2119 (1976).
- 3) J.A. Cowen and W.H. Tantilla, Am. J. Phys. 26, 381 (1958).
- 4) H.M. Gijssman, Ph.D. Thesis, Leiden (1958).
- 5) A.C. Botterman, Ph.D. Thesis, Eindhoven (1976).
- 6) J. Wiebes, W.S. Hulscher and H.C. Kramers, Appl. Sci. Res. 11, 213 (1964-1965).

CHAPTER III

HIGH-TEMPERATURE SUSCEPTIBILITY. †

3.1 Introduction.

In $\text{CoBr}_2 \cdot 6\text{H}_2\text{O}$ all the $[\text{CoBr}_2\text{O}_4]$ -clusters are equivalent and can be described as distorted octahedra. The basal plane contains the four H_2O molecules (XY plane). The Br-Co-Br axis is almost perpendicular to that plane and is slightly elongated (fig. I-1b). From a configuration like this one may expect a crystal field on the magnetic ion with rather strong tetragonal components besides the main term of cubic symmetry. The combined effect of such a crystal field and the spin-orbit coupling results in a splitting of the free-ion ^4F state in a number of levels of which six Kramers doublets are the lowest, as is sketched in fig. III-1. In general it is assumed that at low temperatures, where only the lowest doublet is populated, a description in terms of a fictitious spin $S' = 1/2$, with aniso-

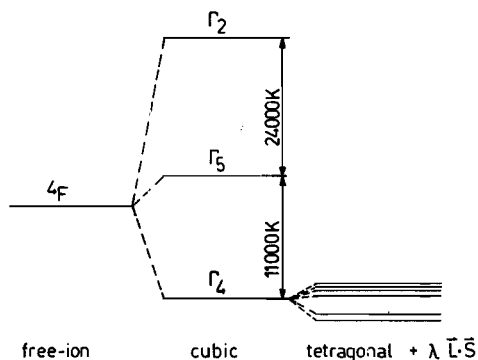


Figure III-1.

Splitting of the Co^{2+} free-ion ground state by a crystal field with tetragonal deviations from cubic symmetry. The energy scale applies to $\text{CoBr}_2 \cdot 6\text{H}_2\text{O}^{5)}$.

†

Part of this chapter was published as :

J.P.A.M. Hijmans, Q.A.G. van Vlimmeren and W.J.M. de Jonge,
 Phys. Rev. B12, 3859 (1975).

tropic exchange parameters and g-values, is sufficient to characterize the magnetic behaviour.

Within this fictitious spin formalism some properties of the exchange tensor can be predicted if the usual assumption is made that the exchange between the real spins is isotropic¹⁾. Projection on to the ground state doublet yields in first order the transformation

$$\vec{S} : = \vec{g}_S \vec{S}' ,$$

where \vec{g}_S is the spin-only g-tensor and \vec{S} the real spin operator. Consequently one has for the exchange interaction the transformation

$$J \vec{S}'_1 \vec{S}'_2 : = J \vec{S}'_1 \vec{g}_{S_1}^T \vec{g}_{S_2}^T \vec{S}'_2 .$$

The crystal symmetry in $\text{CoBr}_2 \cdot 6\text{H}_2\text{O}$ requires $\vec{g}_{S_1} = \vec{g}_{S_2}$, and hence the effective exchange tensor is proportional to \vec{g}_S^2 . As the principal axes of \vec{g}_S coincide with the axes of symmetry of the crystal field, the principal axes of the exchange tensor also coincide with these axes of symmetry.

With the exception of Uryu et al.²⁾, so far the data have been interpreted in terms of the fictitious spin formalism. A detailed survey of the results can be found elsewhere³⁾. The major conclusion is that the magnetic behaviour of $\text{CoBr}_2 \cdot 6\text{H}_2\text{O}$ at low temperatures can be satisfactorily explained on the basis of a square lattice^{††} of $S' = 1/2$ spins with an exchange interaction of the XY type ($J_x = J_y = J, J_z = 0$). This fact is most clearly demonstrated by the values of $g_x \approx g_y \approx 5.0$ and $g_z \approx 2.2$. If one neglects orbital contributions this would yield $J_x \approx J_y$ and $J_z/J_x \approx 0.19$. The quantitative results, however, should be judged with care because in general they are obtained from interpretations imposing a simple model behaviour which will not completely be satisfied. For instance, it is clear that the simple XY model does

††

By a square lattice we mean a lattice with four nearest neighbours and only one interaction \vec{J} . Referring to chapter I, this lattice is characterized by $\vec{J}_1 = \vec{J}$ and $\vec{J}_2 = \vec{0}$.

not account for the non-zero χ_z and the influences of the excited doublet-states. Apart from the direct contribution to the susceptibility at higher temperatures, these excited levels will also give rise to a substantial Van Vleck contribution. In this chapter we will present the susceptibility data up to 120 K and we will show that a consistent set of both crystal field and magnetic parameters quantitatively explains the susceptibility for all three principal directions. The next section will be devoted to the theoretical outline of the procedure. The experimental results will be presented in section 3, whereas we will discuss the results in the final section 4.

3.2 Theory.

The ground state of the $3d^7$ configuration of the Co^{2+} ion is a 4F state ($L = 3, S = 3/2$) while the first excited state is a 4P term ($L = 1, S = 3/2$) at an energy some 20,000 K higher. Usually the assumption is made that the influence of a crystalline environment is small enough to neglect mixing of these states. The relevance of this assumption in this context will be commented later on. As a consequence, the sum over one-electron operators which describes the action of the crystal field can be replaced by an operator depending only on the components of the total angular momentum \vec{L} . This so called "equivalent operator" is normally decomposed in spherical tensor operators $T_q^k(\vec{L})$ ($q = -k, -k+1, \dots, k$) because they possess the same transformation properties as the spherical harmonics Y_k^q occurring in the expansion of the crystal field around the Co nucleus. For instance, an inversion center at the Co position excludes odd k -values in the crystal potential and thus in the equivalent operator. Another correspondence between the T_q^k and Y_k^q results from the fact that we are only dealing with $3d$ ($\ell=2$) electrons. Because $\langle \ell=2, m_\ell | Y_k^q | \ell=2, m'_\ell \rangle = 0$ if $k \geq 5$ no tensor operators with rank $k > 4$ can occur. For a thorough survey of these and other tensor operator properties based on the Wigner-Eckart theorem, the reader is referred to Messiah⁴. One more comment has to be made before we pass on to the details of the calculation. The weights C_q^k of the tensor operators in the Hamiltonian cannot reliably be calculated from the geometry of the ions around Co^{2+} because even a small degree of covalency may have drastic effects on the outcome of any localized electron calculation.

However, the functional form of the hamiltonian must be correct since it depends only on the symmetry of the problem. So, the C_q^k can best be considered as adjustable parameters.

Using the method of operator equivalents the combined effect of a crystal field of orthorhombic symmetry and spin-orbit coupling can be written as:

$$\begin{aligned}
 H = & \frac{1}{2} (C_0^4 + C_4^4) \left[\frac{1}{15} T_0^4 + \frac{1}{6} (T_4^4 + T_{-4}^4) \right] \\
 & + \frac{1}{2} (C_0^4 - C_4^4) \left[\frac{1}{15} T_0^4 - \frac{1}{6} (T_4^4 + T_{-4}^4) \right] + \frac{1}{3} C_0^2 T_0^2 \\
 & + \frac{1}{12} C_2^4 (T_2^4 + T_{-2}^4) + \frac{1}{2} C_2^2 (T_2^2 + T_{-2}^2) + \lambda \vec{L} \cdot \vec{S} ,
 \end{aligned} \tag{1}$$

where

$$\begin{aligned}
 T_0^4 &= 35 L_z^4 - 335 L_z^2 + 360 , \\
 T_{\pm 2}^4 &= (7L_z^2 - 17)L_{\pm}^2 + L_{\pm}^2 (7L_z^2 - 17) , \\
 T_{\pm 4}^4 &= L_{\pm}^4 , \\
 T_0^2 &= 3L_z^2 - 12 , \\
 T_{\pm 2}^2 &= L_{\pm}^2 .
 \end{aligned}$$

In this Hamiltonian the first term represents the cubic field, the next two terms represent the tetragonal field components and the fourth and the fifth terms the orthorhombic field components. In the last term λ is the spin-orbit coupling constant. The z axis is chosen along the tetragonal axis.

In a crystal field of octahedral symmetry the free ion 4F state splits into two orbital triplets Γ_5 and Γ_4 and one orbital singlet Γ_2 , with Γ_4 lowest (fig. III-1). The energy gap between this level and the first excited state Γ_5 is, according to Pappalardo⁵, about 11000 K. For the present we will restrict our attention to the lowest state Γ_4 . A suitable set of orbital basis functions for this ground state is

given by the following combinations of angular momentum functions $|M_L\rangle$ with $L = 3$:

$$\begin{aligned}
 |\alpha_1\rangle &= |0\rangle, \\
 |\alpha_2\rangle &= (\sqrt{10} |3\rangle + \sqrt{6} |-1\rangle)/4, \\
 |\alpha_3\rangle &= (\sqrt{10} |-3\rangle + \sqrt{6} |1\rangle)/4.
 \end{aligned} \tag{2}$$

These orbital states still have a fourfold spin degeneracy. The action of the tetragonal field, the orthorhombic field and the spin-orbit coupling will partially remove this degeneracy and leads to a splitting into six Kramers doublets. A convenient set of product basis functions $|\alpha_i, M_S\rangle$ can be found in

$$\begin{aligned}
 |1\rangle &= |\alpha_1, +3/2\rangle, & |1'\rangle &= |\alpha_1, -3/2\rangle, \\
 |2\rangle &= |\alpha_1, -1/2\rangle, & |2'\rangle &= |\alpha_1, +1/2\rangle, \\
 |3\rangle &= |\alpha_2, -3/2\rangle, & |3'\rangle &= |\alpha_3, +3/2\rangle, \\
 |4\rangle &= |\alpha_2, +1/2\rangle, & |4'\rangle &= |\alpha_3, -1/2\rangle, \\
 |5\rangle &= |\alpha_3, +1/2\rangle, & |5'\rangle &= |\alpha_2, -1/2\rangle, \\
 |6\rangle &= |\alpha_3, -3/2\rangle, & |6'\rangle &= |\alpha_2, +3/2\rangle.
 \end{aligned} \tag{3}$$

On this basis the Hamiltonian (1) factorizes into two identical blocks. The submatrix on the basis $|1\rangle$ through $|6\rangle$ (or on the basis $|1'\rangle$ through $|6'\rangle$) is, apart from a constant diagonal contribution $10C_4^4 + 14C_0^4$,

$$\begin{pmatrix}
 2C_{ax} & 0 & 0 & 0 & \Lambda\sqrt{6} & 0 \\
 0 & 2C_{ax} & 0 & 2\Lambda\sqrt{2} & 0 & \Lambda\sqrt{6} \\
 0 & 0 & -C_{ax} - 3\Lambda & 0 & 0 & C_{or} \\
 0 & 2\Lambda\sqrt{2} & 0 & -C_{ax} + \Lambda & C_{or} & 0 \\
 \Lambda\sqrt{6} & 0 & 0 & C_{or} & -C_{ax} - \Lambda & 0 \\
 0 & \Lambda\sqrt{6} & C_{or} & 0 & 0 & -C_{ax} + 3\Lambda
 \end{pmatrix} \tag{4}$$

The parameters C_{ax} , C_{or} and Λ , introduced in (4), are defined as

$$\begin{aligned} C_{ax} &= 5C_o^4 - 5C_4^4 - 2C_o^2, \\ C_{or} &= 15C_2^4 + 6C_2^2, \\ \Lambda &= 3\lambda/4. \end{aligned} \quad (5)$$

Diagonalization for given values of C_{ax} , C_{or} and Λ yields the eigenvalues $E_{j,i}^o$, where $i = 1,2$ denotes the double degeneracy arising from the existence of the two identical blocks mentioned before. It should be noted that more elaborate calculations, which involve for instance ${}^4P - {}^4F$ mixing under the action of the cubic field, result in the same matrix (4) accompanied by more complicated definitions (3) and (5). Because we will consider C_{ax} , C_{or} and λ as adjustable parameters we do not go into such details.

In order to obtain the zero field susceptibility we have to calculate the effect of a perturbation of the form

$$H_{Zeeman} = \mu_B (k_o L_\alpha + 2S_\alpha) H_\alpha, \quad (6)$$

where μ_B is the Bohr magneton, k_o is taken as a constant, called the orbital reduction factor, which we will discuss later on and the subscript α denotes x , y or z .

The perturbed energy levels can be written as

$$\begin{aligned} E_{j,1} &= E_j^o + f_j^\alpha H + s_j^\alpha H^2 + \dots, \\ E_{j,2} &= E_j^o - f_j^\alpha H + s_j^\alpha H^2 + \dots, \end{aligned} \quad (7)$$

where f_j^α and s_j^α follow from perturbation theory. The doublet g values are found from $g_j^\alpha = 2f_j^\alpha/\mu_B$ and they depend on the orientation of the magnetic field. The spin-only g values, g_S , are found by inserting $k_o = 0$ in (6). From thermodynamics it follows that

$$\chi_\alpha = - \left(\frac{\partial^2 G}{\partial H_\alpha^2} \right)_{H_\alpha=0}, \quad (8)$$

$$\text{where } G = -kT \ln Z \quad (9)$$

$$\text{and } Z = \sum_{j,i} \exp(-E_{j,i}/kT). \quad (10)$$

Combining (7), (8), (9) and (10) we obtain for the susceptibility per spin:

$$\chi_{\alpha} = \frac{1}{Z_0^d} \sum_j \frac{(f_j^{\alpha})^2}{kT} \exp(-E_j^0/kT) - \frac{1}{Z_0^d} \sum_j 2 s_j^{\alpha} \exp(-E_j^0/kT), \quad (11)$$

with

$$Z_0^d = \sum_j \exp(-E_j^0/kT) .$$

The first term in (11) can be considered as a Curie-like susceptibility whereas the second term is known as the Van Vleck contribution χ_{vv} .

So far we have not considered the exchange interaction between neighbouring ions. In view of the fact that the splitting between the ground state doublet and the first excited doublet (which is of the order of 100 K) is at least one order of magnitude larger than the exchange energy, it seems reasonable to treat the exchange interaction as a small perturbation. Therefore, we will consider the exchange contribution only within the groundstate doublet, where it can conveniently be calculated adopting a fictitious $S' = 1/2$ formalism and using the anisotropic g values obtained from the crystal-field calculations outlined before. The fact that this approximation (which implies that only the ground state is populated) does not hold at temperatures comparable with the doublet-doublet splitting introduces only minor errors because the contribution of the exchange interaction at those temperatures is almost negligible.

The interaction between neighbouring spins can be written as:

$$H_{\text{exch}} = -2 \sum_{i < j} (J_x S_i^x S_j^x + J_y S_i^y S_j^y + J_z S_i^z S_j^z) . \quad (12)$$

In our case we assume that the principal axes x, y, z of the exchange tensor \vec{J} coincide with the crystal-field axes, an assumption which is almost exact if dipolar interactions are small and the exchange between real spins is isotropic. The contribution of (12) to the susceptibility is not known to a sufficient degree of accuracy, therefore we have to adopt simplifications which transform (12) into a "model" Hamiltonian from which the contribution is known more accurately. For the susceptibility along the z direction (χ_z)

we will use the high temperature expansion (HTE) of an uniaxial model on a square lattice for which

$$H'_{\text{exch}} = - 2 \sum_{i < j} [J_z S_i^z S_j^z + J_{xy} (S_i^x S_j^x + S_i^y S_j^y)] , \quad (13)$$

where $J_{xy} = J_x = J_y$. For the susceptibility along the x or y axis (χ_x resp. χ_y) we will use the HTE of the pure XY model, also on a square lattice, for which

$$H''_{\text{exch}} = - 2 J_{xy} \sum_{i < j} (S_i^x S_j^x + S_i^y S_j^y) . \quad (14)$$

We calculated χ_z for an exchange interaction according to (13) by the finite cluster expansions method⁶⁾. The results agree completely with those reported by Obokata et al.⁷⁾.

$$\chi_z T / C_z = 1 + \sum_{n=1}^7 \frac{1}{n!} \left(\frac{1}{kT} \right)^n \sum_{j=0}^{[n/2]} (-1)^j C_{nj} J_z^{n-2j} J_{xy}^{2j} , \quad (15)$$

Table III-1.

Numerical value of the coefficients C_{nj} occurring in the high temperature series for χ_z given in formula 15.

j n	0	1	2	3
1	2			
2	6	2		
3	26	18		
4	138	132	20	
5	902	1110	350	
6	6876	10194	4143	458
7	60566	105630	54838	11396

with $C_z = N g_z^2 \mu_B^2 / 4$ and $[n/2]$ denoting $n/2$ if n is even and $(n-1)/2$ if n is odd. The coefficients C_{nj} are given in table III-1. The useful range of such a series expansion can be found from a comparison with the results of the well known Padé approximant method⁸⁾. This technique yields analytical continuations of the HTE which are expected to describe the physical quantity under consideration more accurately than the HTE itself, especially at lower temperatures. In this way it showed that for $J_z/J_{xy} < 0.25$ the HTE can be used up to $|J_{xy}|/kT = 0.5$ (error $< 1\%$).

For χ_x and χ_y de Jongh et al.⁹⁾ reported a formula equivalent with

$$\begin{aligned} \chi_\alpha T/C_\alpha = & 1 + 2K + 8/3 K^2 + 19/6 K^3 + 101/30 K^4 \\ & + 1223/360 K^5 + 1709/504 K^6 \\ & + 3799/1120 K^7 + 15619/5040 K^8 \\ & + 330019/120960 K^9, \end{aligned} \quad (16)$$

where $C_\alpha = N g_\alpha^2 \mu_B^2 / 4$, $K = J_{xy}/(kT)$ and α denotes x or y .

From the average of the Padé approximants of (16) we obtained the following mathematical expression which is valid for negative K up till $|K| = 0.8$ with an error $< 2\%$:

$$\begin{aligned} \chi_\alpha T/C_\alpha = & (1 - 9K/10)^{-3/2} \times \\ & (1 + 0.6500 K + 0.2704 K^2 + 0.2197 K^3 \\ & + 0.0082 K^4 - 0.0267 K^5 \\ & + 0.0300 K^6 + 0.0462 K^7). \end{aligned} \quad (17)$$

3.3 Experimental results.

The susceptibility was measured in the temperature range from 1 K - 120 K along the x , y and z principal axes defined in fig. III-2. The majority of the data points was obtained by a dynamic mutual inductance method which is described in chapter II. The measuring device was constructed in such a way that the crystal could be rotated and also could be moved out of the coil system in order to correct for an empty apparatus effect. In the temperature ranges 1-5 K, 14-20 K, 65-77 K and at 116 K the data were supplemented with absolute static values for χ obtained with a

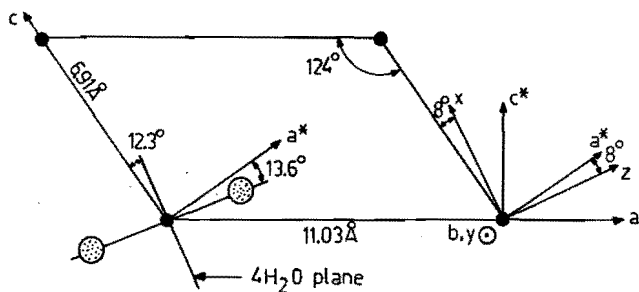


Figure III-2.

Sketch of the ac plane of $\text{CoBr}_2 \cdot 6\text{H}_2\text{O}$ showing the principal axes x , y , z of the susceptibility tensor and the orientation of the $[\text{CoBr}_2\text{O}_4]$ clusters (a^*1c , c^*1a). Cobalt atoms are small and black while bromine atoms are shaded.

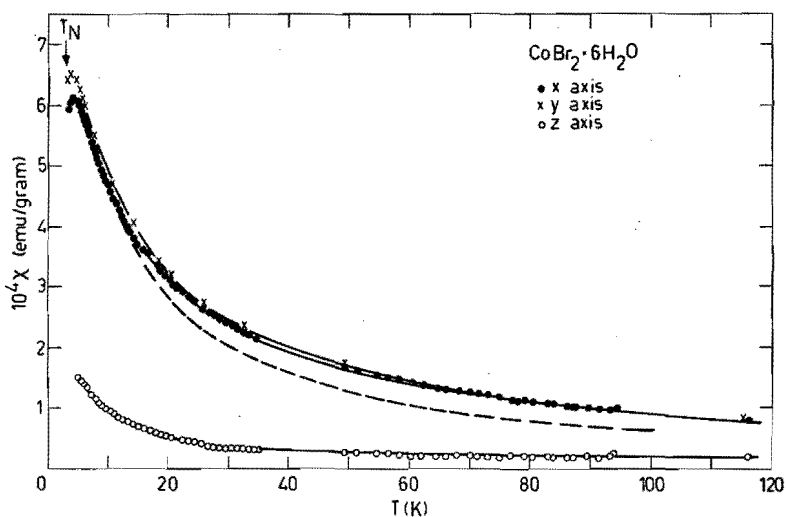


Figure III-3.

Susceptibilities of $\text{CoBr}_2 \cdot 6\text{H}_2\text{O}$ versus temperature. For the y axis only part of the data is shown. The fully drawn curves are calculated with $k_0 = 0.90$, $C_{ax} = -815$ K, $C_{or} = 26$ K, $\lambda = -284$ K, $J_{xy} = -2.37$ K and $J_z = -0.7$ K. The dashed curve represents the extension of the fit for the x axis obtained by de Jongh et al.⁹⁾

Faraday balance. The results are shown in figs. III-3 and III-4 and are tabulated in table III-2. After applying a correction for diamagnetism ($- 5 \times 10^{-7}$ emu/gram), the temperature dependences of χ_x and χ_y ($3.5 \text{ K} < T < 120 \text{ K}$) and χ_z ($5 \text{ K} < T < 120 \text{ K}$) were simultaneously fitted to a combination of expressions (11) and (17), and (15), respectively, with λ , C_{ax} , C_{or} , J_{xy} and J_z as variables. It should be noted that the first (paramagnetic) term in (15) and (16) has to be omitted because it is already contained in (11).

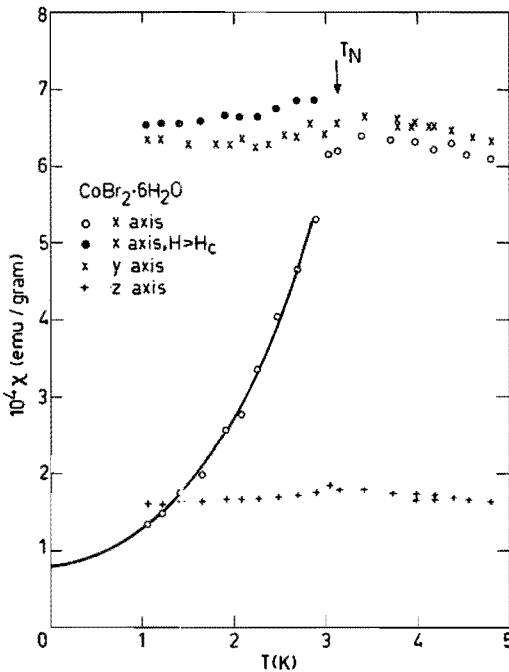


Figure III-4.

Static susceptibilities of $\text{CoBr}_2 \cdot 6\text{H}_2\text{O}$ below $T = 5 \text{ K}$. The drawn curve is used to extrapolate the parallel susceptibility in the ordered state to $T = 0 \text{ K}$ as described in the text.

This procedure was performed with different values of the orbital reduction factor k_o defined in (6).

The influence of this factor on the obtained best-fit magnetic parameters was very small and well within the estimated uncertainty. The deviation between the data points and the calculated points was in all cases comparable with the estimated error in the data points. The resulting magnetic parameters for the ground state are tabulated in table III-3.

Table III-2a.

Experimental data for the susceptibility of $\text{CoBr}_2 \cdot 6\text{H}_2\text{O}$ along the principal axes x , y , z measured with a Faraday balance. Temperatures are given in Kelvin and susceptibilities in units of 10^{-4} emu/gram.

T	χ_x	T	χ_y	T	χ_z
1.22	1.48	1.21	6.35	1.22	1.61
1.41	1.74	1.50	6.29	1.41	1.62
1.66	1.98	1.81	6.28	1.66	1.63
1.92	2.57	1.97	6.28	1.92	1.66
2.08	2.76	2.10	6.36	2.08	1.65
2.27	3.34	2.25	6.24	2.27	1.66
2.48	4.04	2.39	6.28	2.48	1.68
2.70	4.65	2.55	6.41	2.70	1.71
2.90	5.30	2.70	6.39	2.90	1.74
3.05	6.16	2.85	6.54	3.05	1.82
3.16	6.21	2.99	6.40	3.16	1.77
3.42	6.41	3.15	6.57	3.42	1.76
3.73	6.34	3.45	6.65	3.73	1.73
4.00	6.32	3.79	6.52	4.00	1.71
4.20	6.20	3.80	6.60	4.00	1.65
4.21	6.22	3.97	6.51	4.20	1.69
4.40	6.31	4.00	6.55	4.21	1.64
4.61	6.13	4.17	6.51	4.40	1.67
4.82	6.08	4.20	6.50	4.61	1.64
14.08	3.83	4.41	6.45	4.82	1.61
15.38	3.65	4.63	6.37	14.08	0.73
18.49	3.26	4.85	6.31	15.38	0.68
20.30	3.07	14.04	4.03	16.71	0.63
63.42	1.38	16.03	3.67	18.49	0.57
66.84	1.32	17.93	3.47	20.30	0.53
70.31	1.27	20.33	3.20	63.42	0.24
73.47	1.24	63.64	1.46	66.84	0.24
77.19	1.20	67.77	1.39	70.31	0.24
116.00	0.84	71.57	1.34	73.47	0.24
		76.52	1.26	77.19	0.25
		115.20	0.86	116.00	0.20

Table III-2b.

Experimental data for the susceptibility of $\text{CoBr}_2 \cdot 6\text{H}_2\text{O}$ along the principal axes x , y , z obtained by a mutual inductance method. Temperatures are given in Kelvin and susceptibilities in units of 10^{-4} emu/gram.

T	χ_x	T	χ_y	T	χ_z
3.96	6.14	4.00	6.49	3.96	1.67
4.14	6.12	4.22	6.48	4.14	1.64
4.22	6.13	4.24	6.48	4.22	1.66
4.26	6.14	4.31	6.51	4.26	1.66
4.41	6.13	4.37	6.49	4.41	1.64
4.63	6.11	4.57	6.42	4.63	1.58
4.87	6.09	4.76	6.39	4.87	1.56
5.04	6.05	4.93	6.29	5.04	1.51
5.27	5.99	5.08	6.28	5.27	1.51
5.46	5.94	5.24	6.22	5.46	1.48
5.69	5.86	5.45	6.19	5.69	1.43
5.99	5.79	5.54	6.05	5.99	1.42
6.16	5.75	5.66	6.09	6.16	1.37
6.36	5.71	6.08	5.97	6.36	1.35
6.65	5.60	6.33	5.86	6.65	1.30
6.89	5.54	6.53	5.79	6.89	1.28
7.24	5.37	6.90	5.72	7.24	1.22
7.51	5.30	7.22	5.61	7.51	1.15
7.84	5.22	7.52	5.49	7.84	1.15
8.12	5.11	7.90	5.37	8.12	1.11
8.43	5.04	8.16	5.32	8.43	1.09
8.74	4.92	8.28	5.29	8.74	1.05
9.05	4.86	8.42	5.22	9.05	1.03
9.46	4.76	8.69	5.03	9.46	1.00
9.78	4.72	9.08	4.93	9.78	0.99
10.24	4.59	9.39	4.93	10.24	0.95
10.76	4.48	9.71	4.77	10.76	0.92
11.17	4.39	10.01	4.70	11.17	0.89
11.78	4.27	10.54	4.61	11.78	0.83
12.13	4.18	11.03	4.52	12.13	0.82
12.55	4.08	11.48	4.43	12.55	0.80
13.16	3.99	12.05	4.30	13.16	0.79
13.68	3.90	12.40	4.20	13.68	0.75
14.13	3.81	12.95	4.11	14.13	0.73
14.24	3.89	13.55	4.08	14.24	0.74
14.75	3.80	14.20	3.91	14.75	0.71
14.82	3.71	14.24	4.08	14.82	0.68
15.27	3.72	14.87	3.83	15.27	0.67
15.84	3.60	15.35	3.87	15.84	0.68
15.96	3.55	16.28	3.75	15.96	0.67
16.50	3.54	16.57	3.58	16.50	0.67
17.10	3.42	17.30	3.57	17.10	0.62
17.28	3.36	18.32	3.42	17.28	0.63
17.96	3.33	19.35	3.37	17.96	0.60
18.66	3.25	20.46	3.22	18.66	0.56
19.47	3.17	21.41	3.20	19.47	0.57
20.40	3.11	22.50	3.10	20.75	0.53
20.75	3.04	23.44	2.97	20.40	0.55
21.40	2.95	24.56	2.91	22.45	0.51
22.45	2.92	25.50	2.85	23.44	0.47
23.44	2.84	26.40	2.75	24.35	0.46
24.35	2.75	27.40	2.68	25.60	0.42
25.60	2.66	28.40	2.62	26.63	0.40
26.63	2.58	29.30	2.55	27.48	0.40
27.48	2.54	30.50	2.51	28.50	0.39
28.50	2.48	31.53	2.44	29.50	0.39
29.50	2.42	32.41	2.38	30.40	0.38

(Continued overleaf)

Table III-2b (continued).

T	χ_x	T	χ_y	T	χ_z
30.40	2.37	33.45	2.36	31.50	0.36
31.50	2.32	34.33	2.31	32.32	0.35
32.32	2.25	49.30	1.73	33.40	0.34
33.40	2.22	49.40	1.66	34.15	0.35
34.15	2.19	49.50	1.82	35.62	0.34
34.50	2.17	52.55	1.59	49.25	0.29
49.25	1.70	52.70	1.63	51.45	0.28
51.45	1.64	56.50	1.55	54.65	0.27
54.65	1.56	56.70	1.63	56.40	0.26
56.40	1.53	59.25	1.52	58.25	0.25
58.25	1.49	60.25	1.48	60.30	0.24
60.30	1.44	61.70	1.46	62.10	0.25
62.10	1.42	62.85	1.46	64.60	0.24
64.60	1.36	64.30	1.46	65.95	0.23
65.95	1.33	64.40	1.38	68.20	0.25
68.20	1.32	65.55	1.38	70.10	0.25
70.10	1.30	66.00	1.40	71.40	0.24
71.40	1.29	66.60	1.42	71.50	0.16
71.50	1.26	66.90	1.42	73.05	0.22
73.05	1.25	67.70	1.40	75.00	0.22
75.00	1.24	68.10	1.39	77.00	0.24
77.00	1.22	68.45	1.40	77.10	0.17
77.10	1.17	69.25	1.36	77.60	0.25
77.60	1.15	70.35	1.29	79.10	0.23
79.10	1.17	70.40	1.23	80.50	0.23
80.50	1.16	71.80	1.30	83.00	0.23
83.00	1.14	71.90	1.32	83.90	0.24
83.90	1.12	73.40	1.26	86.20	0.21
86.20	1.06	73.80	1.28	86.80	0.25
86.80	1.06	76.00	1.23	87.30	0.24
87.30	1.06	76.05	1.25	89.40	0.24
89.40	1.06	77.20	1.13	91.40	0.21
91.40	1.01	77.90	1.16	93.30	0.23
93.30	1.02	78.80	1.18	94.05	0.28
94.05	1.04	80.70	1.18		
		82.40	1.16		
		82.80	1.03		
		84.00	1.16		
		86.60	1.15		
		90.40	1.06		
		94.00	1.08		
		95.50	1.03		

In table III-4 the best-fit crystal-field parameters are tabulated as a function of the orbital reduction factor k_o and in fig. III-5 several quantities are plotted as a function of C_{ax} . It can be seen that the tetragonal distortion and the spin-orbit coupling are rather sensitive to a change of k_o . This leaves, however, the lowest doublet-doublet splitting (E_1) almost unaffected. This, combined with the fact that the splitting of the doublets reflects the strong axial field such that there is a large energy gap between the lowest two doublets and the centre of the four others (E_g), explains why in the temperature range we studied the magnetic parameters are only slightly affected by the reduction factor k_o .

Table III-3.

Best-fit magnetic parameters and related quantities for the Co^{2+} ground state in $\text{CoBr}_2 \cdot 6\text{H}_2\text{O}$. For χ_{VV} the temperature independent value below 35 K is given.

Quantity	This work	Literature	Quantity	This work
J_{xy} (K)	-2.37 ± 0.05	$-2.45 \pm 0.1^{9)}$	$\chi_{\text{VVx,y}}$ (emu/gr)	$(6 \pm 1) \times 10^{-5}$
J_z (K)	-0.7 ± 0.1	$-0.4 \pm 0.1^{3)}$	χ_{VVz} (emu/gr)	$(1.2 \pm 0.5) \times 10^{-6}$
g_x	4.70 ± 0.05	$5.1^{12)}$ $5.0 \pm 0.1^{9)}$	g_{Sx}	3.90 ± 0.05
g_y	4.82 ± 0.05	$5.0^{12)}$ $5.0 \pm 0.1^{9)}$	g_{Sy}	3.99 ± 0.05
g_z	2.02 ± 0.05	$2.2^{12)}$	g_{Sz}	2.01 ± 0.05

Table III-4.

Best-fit crystal-field parameters as a function of the orbital reduction factor k_o . Also given are the resulting values of E_1 , E_g (see text) and the overall width ΔE of the four highest doublet energies.

k_o	C_{ax} (K)	C_{or} (K)	λ (K)	E_1 (K)	E_g (K)	ΔE (K)
1.00	-1140	34	-336	177	3790	1430
0.95	-970	30	-312	177	3290	1310
0.90	-815	26	-284	177	2810	1190
0.85	-680	22	-256	173	2390	1060

3.4 Discussion.

In table III-3 some results for the magnetic parameters from previous sources are also given. The main reason for the discrepancies, in particular for the g values, can be found in the Van Vleck contribution. According to our calculations this contribution amounts to $\sim 10\%$ of the total experimental susceptibility in the temperature region between 3.5 K and 15 K, studied by previous authors³⁾. As a

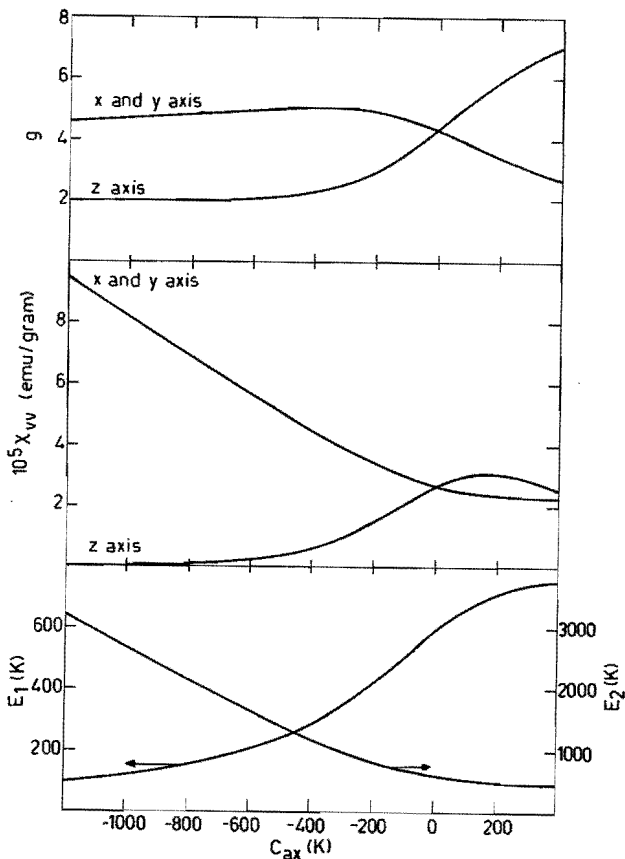


Figure III-5.

Various dependences on C_{ax} calculated with $k_0 = 1$, $C_{or} = 0$ K and $\lambda = -260$ K. From top to bottom: the g values, the value of the Van Vleck contribution χ_{VV} for $T \rightarrow 0$ K and the energies of the first and second excited doublet state measured from the groundstate.

check on this number we extrapolated the $\chi_{//} = \chi_x$ in the ordered state to $T = 0$ K, taking into account that, according to spin-wave theory¹⁰⁾, the low-temperature expansion of χ does not contain a first power term in T . This extrapolation is shown in fig. III-4 and results in $\chi_{vvx} = (8 \pm 1) \times 10^{-5}$ emu/gram, which value may be compared with the calculated $\chi_{vvx,y} = (6 \pm 1) \times 10^{-5}$ emu/gram. To demonstrate the influence of this and other crystal-field effects we have reproduced the theoretical fit obtained by De Jongh et al.⁹⁾ from the temperature dependence of $\chi_{x,y}$ below $T = 15$ K in fig. III-3.

Inspection of table III-3 also shows that the ratio J_z/J_{xy} is substantially higher than estimated before³⁾. The reason for this is that former estimates were obtained from the anisotropy in the g tensor, neglecting orbital contributions. The orbital contribution to g_z is rather small but to $g_{x,y}$ it is substantial. This tends to change the exchange anisotropy drastically. In our case we obtain for $(g_{S_z}/g_{S_x})^2 = 0.27 \pm 0.02$ and independently $J_z/J_{xy} = 0.29 \pm 0.04$, which is in rather fair agreement.

It was our aim to interpret the susceptibility data with a minimum of conditions imposed upon the system. We could not obtain, however, independent information about J_x and J_y because in our procedure we were limited by the available solutions of model Hamiltonians, and had to assume $J_x = J_y$. The quoted value for J_{xy} should therefore be considered as an average of J_x and J_y . If one adapts the view that $J_x/J_y = (g_{S_x}/g_{S_y})^2$ we arrive at $J_x/J_y = 0.96 \pm 0.05$ which seems to justify the conjecture $J_x = J_y$.

As we noted before the crystal-field parameters, tabulated in table III-4, reflect the strong axial symmetry. Comparison of these data with those obtained by Uryu et al.²⁾ from their calculation of the Schottky anomaly in the specific heat, is hampered by the fact that they have chosen the z -axis of the system along the b -axis. In their treatment the axial symmetry around the Br-Co-Br axis seems purely accidental and is caused by the combination of a tetragonal term and an orthorhombic term which are of roughly the same order of magnitude. The energy levels were obtained with an assumed fixed spin-orbit coupling of -140 cm^{-1} (-201 K) and are quite different from our results. One should, however, bear in mind that their results were obtained from a rather qualitative comparison with experimental data which exhibit rather large uncertainties.

In eq. (6) we introduced the orbital reduction factor k_o . Formally this type of factor is defined by¹¹⁾

$$k_{ij} = \langle \psi_i | \vec{\ell} | \psi_j \rangle / \langle d_i | \vec{\ell} | d_j \rangle , \quad (18)$$

where $\vec{\ell}$ is the one-electron orbital angular momentum operator, the ψ 's are the molecular orbitals of the cluster and the d 's are the corresponding 3d orbitals. Now the reduction depends on magnitude and origin of the spin density transferred to the ligand. In typical cases k_o varies from ~ 0.8 to 1.0 for transition-metal ions in ionic salts. This range has been chosen for table III-4. Smaller k_o values give rise to a slightly worse fit to the susceptibility data. As we noted before the best-fit tetragonal term and the spin-orbit coupling are rather sensitive to k_o . As there is no significant change in the quality of the fit we have no way to decide about these values. As far as the spin-orbit coupling is concerned the values in table III-4 are, on the average, in absolute value higher than the free-ion value -260 K. Owing to the covalency in the bonding of the central ion with the ligands and the spin-orbit coupling on the ligand a modification of the free-ion value can be anticipated. Typically in the transition metal complexes studied so far, this amounts to a reduction of the free-ion value. However, as pointed out by Owen and Thornley¹¹⁾, this strongly depends on the symmetry of the bond and the ligand ion. More specifically they state that heavy ligands (with large spin-orbit coupling), such as Br^- , might give an effective $|\lambda|$ larger than the free-ion value. Though the value of $|\lambda|$ in this case is rather high on the average it does not seem to be inconsistent with theoretical predictions. Moreover, the experimental values reported in Co^{++} salts seem to be restricted to cubic cases while we are dealing with a strong tetragonal distortion.

3.5 References.

- 1) P.W. Anderson, *Solid State Physics*, Vol. XIV (Academic Press 1963).
- 2) N. Uryu, J. Skalyo and S.A. Friedberg, *Phys. Rev.* 144, 689 (1966).
- 3) J.W. Metselaar, L.J. de Jongh and D. de Klerk, *Physica* 79B, 53 (1975).
- 4) A. Messiah in *Quantum Mechanics*, Vol. II, North-Holland Publishing Company, Amsterdam 1970.
- 5) R. Pappalardo, *Phil. Mag.* 4, 219 (1959).
- 6) G.S. Rushbrooke, G.A. Baker, Jr., and P.J. Wood in *Phase Transitions and Critical Phenomena*, Vol. III, Edited by C. Domb and M.S. Green, Academic Press, London 1974.
- 7) T. Obokata, I. Ono and T. Oguchi, *J. Phys. Soc. Japan* 23, 1327 (1967).
- 8) D.S. Gaunt and A.J. Gutman in *Phase Transitions and Critical Phenomena*, Vol. III, Edited by C. Domb and M.S. Green, Academic Press, London 1974.
- 9) L.J. de Jongh, D.D. Betts and D.J. Austen, *Solid State Comm.* 15, 1711 (1974).
- 10) R. Kubo, *Phys. Rev.* 87, 568 (1952).
- 11) J. Owen and J.H.M. Thornley, *Rep. Progr. Phys.* 29, 675 (1966).
- 12) T.E. Murray and G.K. Wessel, *J. Phys. Soc. Japan* 24, 738 (1968).

CHAPTER IV

SPECIFIC HEAT.

4.1 Introduction.

In this chapter we will present the results of detailed specific heat measurements in the temperature range from 1.2 to 11 K. More or less preliminary specific heat data in the range from 1.65 to 5.05 K were reported by Forstat et al.¹⁾. The data in the paramagnetic state will be compared with high-temperature expansions while the critical behaviour in the vicinity of the ordering temperature will be described in terms of a logarithmic divergence.

4.2 Experimental results.[†]

High precision heat capacity measurements were performed on a sample consisting of 33.038 grams of small crystals of $\text{CoBr}_2 \cdot 6\text{H}_2\text{O}$ (average linear dimension 5 mm). The specimen was sealed inside a simple vacuum calorimeter together with a little ^3He exchange gas. Temperatures were obtained from a calibrated germanium thermometer which was measured with an audiofrequency resistance bridge using synchronous detection as described in chapter II.

The specific heat data between 1.2 K and 11 K are shown in fig. IV-1 and tabulated in table IV-1; the data in the immediate neighbourhood of the ordering temperature ($T_N = 3.150 \pm 0.005$ K) are given more in detail in fig. IV-2. Between 4.5 K and 11 K our data are very well represented by the equation $C/R = AT^3 + BT^{-2}$ with $A = 3.158 \times 10^{-4} \text{ K}^{-3}$ and $B = 5.768 \text{ K}^2$.

The relative RMS error of the fit was less than 3×10^{-3} . We used the inferred value of A to subtract the lattice contribution from the measured specific heat in order to obtain the magnetic contribution.

†

Part of this section was published in:
K. Kopinga, P.W.M. Borm and W.J.M. de Jonge,
Phys. Rev. B10, 4690 (1974).

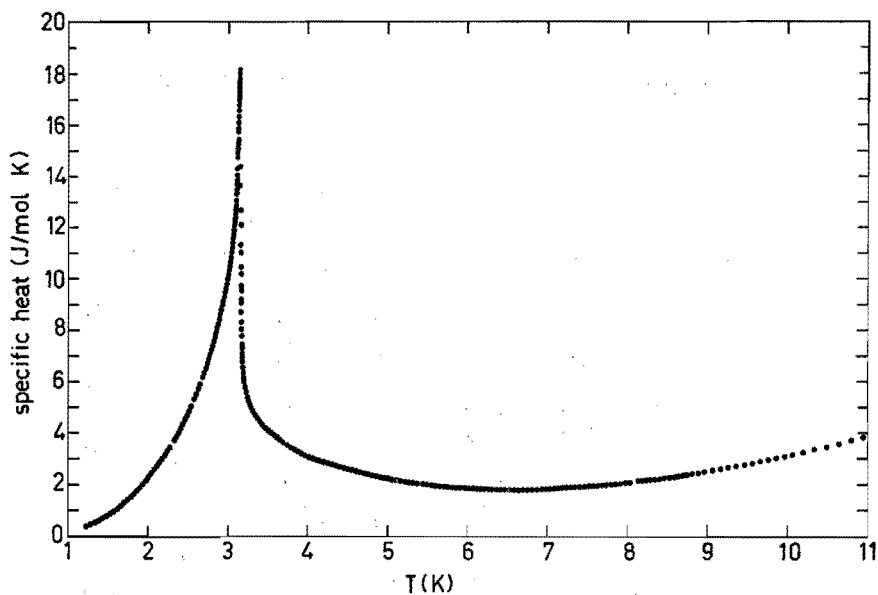


Figure IV-1.

Molar specific heat of $\text{CoBr}_2 \cdot 6\text{H}_2\text{O}$.

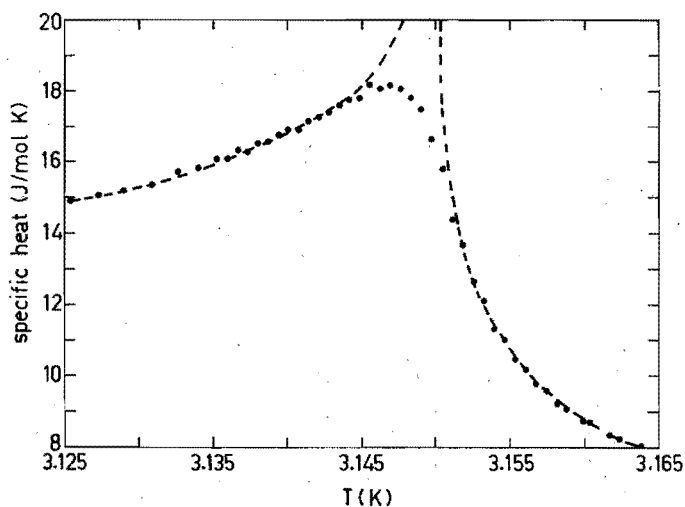


Figure IV-2.

The heat capacity of $\text{CoBr}_2 \cdot 6\text{H}_2\text{O}$ in the immediate neighbourhood of the ordering temperature. The dashed curves correspond to the drawn lines in figure IV-5.

Table IV-1.

Experimental specific heat of $\text{CoBr}_2 \cdot 6\text{H}_2\text{O}$. Temperatures are given in Kelvin and specific heat values in J/mol K.

T	C	T	C	T	C	T	C
1.225	.389	2.675	6.155	3.077	12.133	3.160	8.696
1.246	.421	2.695	6.303	3.081	12.265	3.161	8.319
1.289	.485	2.720	6.458	3.086	12.441	3.162	8.191
1.324	.525	2.729	6.645	3.090	12.628	3.163	8.021
1.339	.548	2.740	6.631	3.094	12.822	3.165	7.766
1.374	.604	2.749	6.843	3.099	13.023	3.166	7.623
1.394	.637	2.760	6.838	3.103	13.303	3.167	7.431
1.423	.697	2.773	6.953	3.108	13.475	3.169	7.308
1.445	.725	2.780	7.029	3.110	13.673	3.170	7.192
1.473	.790	2.790	7.153	3.112	13.802	3.172	7.089
1.494	.855	2.800	7.240	3.114	13.948	3.173	6.983
1.523	.870	2.809	7.360	3.116	14.029	3.175	6.897
1.547	.883	2.820	7.464	3.119	14.303	3.176	6.813
1.573	.985	2.829	7.586	3.121	14.740	3.177	6.750
1.595	.998	2.840	7.685	3.123	14.733	3.179	6.666
1.623	1.107	2.849	7.816	3.125	14.911	3.182	6.541
1.644	1.126	2.860	7.945	3.127	15.071	3.185	6.431
1.674	1.258	2.869	8.058	3.129	15.205	3.189	6.304
1.694	1.265	2.880	8.183	3.130	15.386	3.195	6.143
1.725	1.403	2.889	8.339	3.132	15.742	3.201	5.993
1.744	1.417	2.897	8.410	3.134	15.848	3.207	5.872
1.775	1.555	2.905	8.553	3.135	16.092	3.212	5.774
1.795	1.566	2.909	8.591	3.136	16.116	3.218	5.692
1.825	1.693	2.915	8.697	3.136	16.332	3.225	5.584
1.845	1.727	2.919	8.747	3.137	16.279	3.235	5.480
1.877	1.819	2.925	8.816	3.138	16.529	3.245	5.369
1.895	1.911	2.929	8.892	3.138	16.597	3.255	5.263
1.927	1.997	2.935	8.960	3.139	16.765	3.265	5.176
1.948	2.011	2.939	9.042	3.140	16.921	3.275	5.093
1.977	2.180	2.945	9.136	3.140	16.920	3.285	5.019
1.998	2.209	2.949	9.215	3.141	17.146	3.295	4.954
2.027	2.393	2.954	9.298	3.142	17.256	3.295	4.941
2.047	2.431	2.959	9.353	3.142	17.422	3.307	4.862
2.077	2.603	2.964	9.462	3.143	17.602	3.322	4.775
2.104	2.568	2.969	9.560	3.144	17.752	3.337	4.688
2.127	2.794	2.974	9.600	3.144	17.797	3.352	4.615
2.146	2.750	2.979	9.772	3.145	18.162	3.367	4.545
2.174	3.062	2.984	9.839	3.146	18.057	3.382	4.481
2.195	2.970	2.989	9.923	3.146	18.166	3.397	4.421
2.224	3.347	2.995	10.016	3.147	18.060	3.412	4.362
2.244	3.215	2.999	10.132	3.148	17.808	3.430	4.299
2.273	3.396	3.004	10.220	3.149	17.483	3.450	4.231
2.294	3.478	3.009	10.319	3.149	16.649	3.470	4.166
2.330	3.705	3.014	10.443	3.150	15.818	3.490	4.107
2.344	3.766	3.019	10.558	3.151	14.378	3.510	4.051
2.375	3.966	3.025	10.660	3.151	13.658	3.530	3.995
2.395	4.062	3.029	10.795	3.152	12.658	3.550	3.940
2.425	4.271	3.034	10.902	3.153	12.106	3.570	3.890
2.444	4.380	3.039	11.030	3.153	11.313	3.590	3.840
2.475	4.598	3.044	11.151	3.154	11.016	3.615	3.784
2.494	4.711	3.049	11.305	3.155	10.446	3.645	3.718
2.525	4.951	3.052	11.348	3.156	10.190	3.675	3.659
2.545	5.083	3.056	11.438	3.156	9.748	3.705	3.598
2.575	5.312	3.060	11.560	3.157	9.555	3.735	3.541
2.595	5.479	3.064	11.678	3.158	9.200	3.765	3.488
2.625	5.704	3.069	11.823	3.158	9.068	3.795	3.437
2.645	5.867	3.073	11.973	3.159	8.703	3.825	3.387

Table IV-1 (continued).

T	C	T	C	T	C	T	C
3.855	3.335	4.815	2.372	6.134	1.878	7.924	2.073
3.885	3.288	4.845	2.345	6.184	1.873	7.973	2.095
3.915	3.245	4.875	2.326	6.234	1.871	8.024	2.105
3.945	3.204	4.905	2.315	6.284	1.874	8.130	2.151
3.975	3.163	4.935	2.293	6.337	1.863	8.174	2.168
4.005	3.126	4.965	2.272	6.392	1.863	8.224	2.182
4.035	3.086	4.995	2.257	6.443	1.861	8.274	2.204
4.064	3.050	5.025	2.243	6.474	1.855	8.324	2.223
4.094	3.019	5.055	2.222	6.524	1.859	8.374	2.242
4.124	2.985	5.085	2.208	6.574	1.855	8.424	2.261
4.154	2.939	5.115	2.193	6.624	1.858	8.474	2.283
4.184	2.921	5.145	2.177	6.674	1.856	8.524	2.306
4.214	2.888	5.175	2.156	6.724	1.857	8.574	2.325
4.244	2.855	5.205	2.146	6.774	1.860	8.624	2.349
4.274	2.832	5.235	2.121	6.824	1.864	8.674	2.377
4.304	2.799	5.265	2.118	6.874	1.864	8.734	2.401
4.334	2.775	5.295	2.108	6.924	1.870	8.807	2.426
4.364	2.746	5.325	2.095	6.974	1.875	8.875	2.466
4.394	2.717	5.355	2.082	7.024	1.882	8.956	2.508
4.424	2.687	5.425	2.048	7.074	1.885	9.051	2.552
4.454	2.666	5.469	2.036	7.124	1.889	9.150	2.611
4.484	2.644	5.510	2.021	7.174	1.898	9.250	2.672
4.514	2.616	5.550	2.005	7.224	1.910	9.350	2.728
4.544	2.583	5.590	1.996	7.274	1.919	9.451	2.777
4.545	2.554	5.630	1.985	7.324	1.931	9.552	2.835
4.574	2.563	5.670	1.975	7.374	1.936	9.651	2.902
4.575	2.525	5.710	1.963	7.424	1.944	9.751	2.965
4.604	2.538	5.750	1.951	7.474	1.957	9.851	3.026
4.605	2.506	5.790	1.943	7.524	1.968	9.951	3.097
4.634	2.522	5.830	1.929	7.574	1.985	10.050	3.162
4.635	2.491	5.870	1.924	7.624	1.996	10.175	3.250
4.665	2.467	5.909	1.915	7.674	2.008	10.325	3.369
4.695	2.444	5.949	1.907	7.724	2.022	10.475	3.471
4.725	2.425	5.989	1.902	7.774	2.032	10.624	3.590
4.755	2.407	6.034	1.892	7.824	2.046	10.775	3.708
4.785	2.388	6.084	1.887	7.874	2.058	10.925	3.823

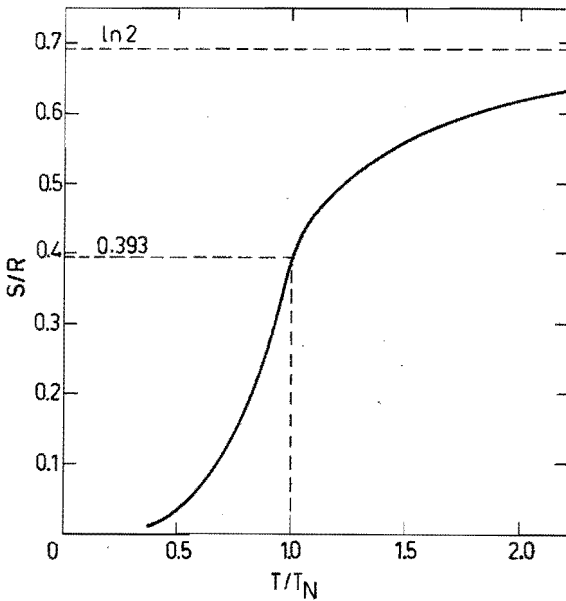


Figure IV-3.

The magnetic entropy of $\text{CoBr}_2 \cdot 6\text{H}_2\text{O}$ in the temperature range $1.2 \text{ K} < T < 7.0 \text{ K}$.

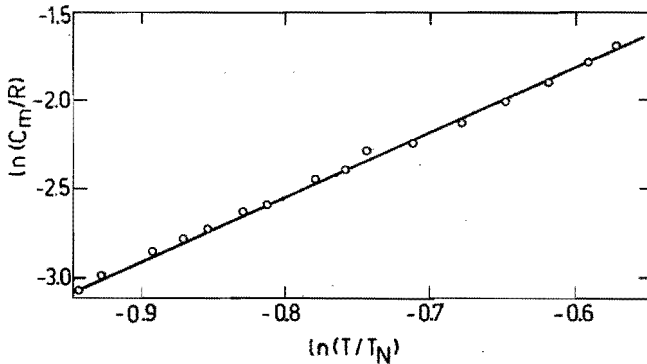


Figure IV-4.

Low temperature behaviour ($1.2 \text{ K} < T < 1.8 \text{ K}$) of the magnetic specific heat of $\text{CoBr}_2 \cdot 6\text{H}_2\text{O}$.

The straight line corresponds to the powerlaw $\frac{C_m}{R} = 1.54 \left(\frac{T}{T_N} \right)^{3.72}$.

In fig. IV-3 the magnetic entropy is plotted versus temperature. The total magnetic entropy increase was found to be 0.690 R, which agrees within 0.4 percent with the theoretical value $R \ln 2$ for an $S = 1/2$ system. An amount of 0.393 R (57%) was gained below the ordering temperature. In all entropy calculations the magnetic specific heat below 1.2 K was represented by $C_m/R = 1.54 (T/T_N)^{3.72}$ because this relation holds between 1.2 and 1.8 K as is evident from fig. IV-4. A summary of the relevant parameters is given in table IV-2 together with our results for the deuterated (98% D_2O) compound.

Fig. IV-5 shows a plot of C versus $^{10}\log(|T-T_N|/T_N)$ for $T_N = 3.150$ K. With this choice for T_N the heat capacity near the transition point satisfies the equations $C/R = 0.3 - 0.27 \ln((T_N-T)/T_N)$ and $C/R = -0.7 - 0.27 \ln((T-T_N)/T_N)$ for $T < T_N$ and $T > T_N$ respectively. These

Table IV-2.

Parameters inferred from specific heat data for $CoBr_2 \cdot 6H_2O$ and $CoBr_2 \cdot 6D_2O$ (98% D_2O). The coefficients A and B are obtained from fits of the type $C/R = AT^3 + BT^{-2}$ for $T > 4.5$ K. The low temperature behaviour of the magnetic contribution is observed experimentally for $1.2 \text{ K} < T < 1.8 \text{ K}$ and is assumed to be valid also for $T < 1.2 \text{ K}$.

	$CoBr_2 \cdot 6H_2O$	$CoBr_2 \cdot 6D_2O$
T_N (K)	3.150 ± 0.005	3.226 ± 0.005
A (K^{-3})	$(3.16 \pm 0.01) \times 10^{-4}$	$(3.22 \pm 0.01) \times 10^{-4}$
B (K^2)	5.77 ± 0.03	5.56 ± 0.03
Low temperature behaviour	$\frac{C_m}{R} = 1.54 \left(\frac{T}{T_N}\right)^{3.72}$	$\frac{C_m}{R} = 1.56 \left(\frac{T}{T_N}\right)^{3.76}$
Magnetic entropy gained below T_N	$0.57 R \ln 2$	$0.60 R \ln 2$
$\int_0^{\infty} C_m dT$ (J/mol)	23.4 ± 0.1	23.4 ± 0.1

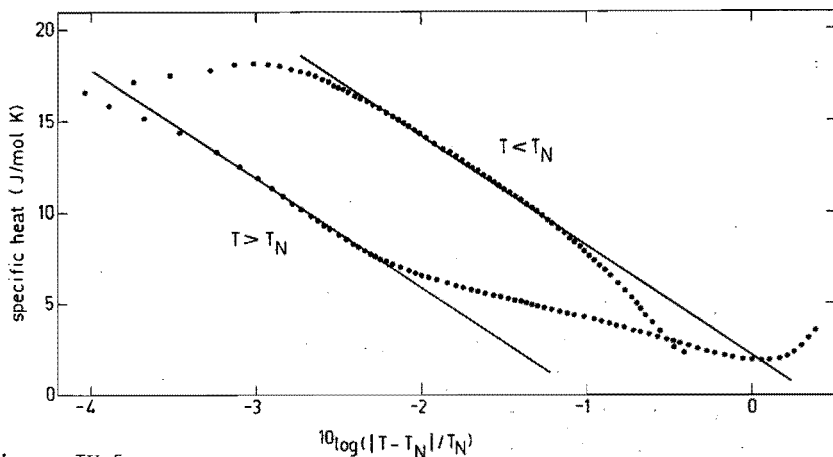


Figure IV-5.

The heat capacity of $\text{CoBr}_2 \cdot 6\text{H}_2\text{O}$ plotted versus $10 \log (|T - T_N|/T_N)$. The drawn lines represent the equations $C/R = 0.3 - 0.27 \ln ((T_N - T)/T_N)$ and $C/R = -0.7 - 0.27 \ln ((T - T_N)/T_N)$ for $T < T_N$ and $T > T_N$, respectively.

equations describe the dashed curves in fig. IV-2. Qualitatively, this behaviour is the same as observed in the specific heat of $\text{CoCl}_2 \cdot 6\text{H}_2\text{O}^{2)}$.

We note that for both the chlorine and the bromine compound the value of T_N that gives the best fit, with the constraint that the coefficient of $\ln(|T - T_N|/T_N)$ is the same below and above T_N , is a few millikelvin higher than the temperature that corresponds with the maximum of the specific heat. This is most likely explained by the significant rounding of the peak (see fig. IV-2), that has been assumed to be mainly due to crystal imperfections²⁾ which may give rise to a small difference in the local exchange interactions.

Concerning the assumed type of divergence at $T = T_N$, the following remarks can be made. A logarithmic singularity in the specific heat at the ordering temperature is displayed by the two-dimensional Ising model³⁾. The ordering of a three-dimensional Ising model may be described by a power law behaviour with a critical exponent $\alpha \approx 0.09 - 0.12$ ^{4,5)}. Calculations based upon high-temperature expansions indicate that the two-dimensional XY-model does not show any singularity in the specific heat^{6,7)}. For the three-dimensional XY-model a critical exponent $\alpha = -0.007 \pm 0.009$ ⁵⁾ has been obtained, which indicates a possible logarithmic behaviour of the specific heat.

4.3 Exchange interactions.

The most direct method to interpret our specific heat data seems to confront them with the calculated magnetic specific heat C_m of the two dimensional square lattice with pure XY interaction as reported by Rogiers et al.⁸⁾, i.e.:

$$C_m/R = K^2 - \frac{1}{4} K^4 - \frac{11}{24} K^6 + \frac{595}{576} K^8 - \frac{9229}{6720} K^{10} + \frac{2202209}{1814400} K^{12} + \dots \quad (1)$$

where $K = J_{xy}/(kT)$ (c.f. chapter III) and R denotes the molar gas constant.

A fit in the temperature region $4.1 \text{ K} < T < 11 \text{ K}$, with eq. 1 representing the magnetic contribution and a lattice contribution of the form AT^3 , yielded $J_{xy}/k = -2.52 \text{ K}$ and $A = 3.075 \times 10^{-4} \text{ K}^{-3}$. We chose 4.1 K as the lowest temperature occurring in the fit because the finite series eq. 1 seems to be reliable only for $|K| < 0.6$. A similar procedure performed by De Jongh et al.⁹⁾ for $\text{CoCl}_2 \cdot 6\text{H}_2\text{O}$ gave $J_{xy} = -2.05 \text{ K}$.

It should be noticed that the procedure outlined above imposes the conditions $J_x = J_y = J_{xy}$, $J_z = 0$ and assumes a perfect square lattice ($J_2 = 0$). Although, qualitatively, these conditions may be reasonably satisfied in this case (c.f. chapter III), we felt the need to see whether or not the available data could be explained without using these simplifications. For instance, in theory one could use the HTE for the specific heat in the case of orthorhombic interactions on a square lattice as developed by De Neef and Hijmans¹⁰⁾, thus dropping the conditions $J_x = J_y$ and $J_z = 0$.

However, as the magnetic specific heat is dominated by a T^{-2} behaviour down to 4.5 K , one cannot expect a meaningful numerical value for the coefficients of the higher inverse powers of T because such a series cannot represent the singularity occurring at $T_N = 3.15 \text{ K}$. On the other hand, the coefficient of T^{-3} must be small because otherwise the influence of this term would show appreciably at 4.5 K as follows from a dominant exchange interaction of $\approx -2.50 \text{ K}$. To obtain quantitative results the experimental data were fitted with the expression

$$C/R = a T^3 + c_2 T^{-2} + c_3 T^{-3}. \quad (2)$$

The procedure was performed for several fixed values of c_3 . A minimum

mean error of 0.27% was obtained for $c_3/c_2 = 0.15$ K and $c_2 = 5.60$ K². For $c_3/c_2 = -0.6$ K and $c_3/c_2 = 1.1$ K the mean error has reached the value of 1% and the fit clearly shows systematic deviations.

The HTE-coefficients c_2 and c_3 for a general lattice of identical spins S with the interaction

$$H = - 2 \sum_{m < n} \sum (J_{mn}^x S_m^x S_n^x + J_{mn}^y S_m^y S_n^y + J_{mn}^z S_m^z S_n^z) \quad (3)$$

can be written as

$$c_2 = \frac{2 S^2 (S+1)^2}{9 k^2} \sum_{m \neq 0} \left\{ (J_{0m}^x)^2 + (J_{0m}^y)^2 + (J_{0m}^z)^2 \right\}, \quad (4)$$

$$c_3 = \frac{2 S^2 (S+1)^2}{9 k^3} \left\{ \frac{4}{3} S(S+1) \times \sum_{m \neq 0} \sum_{n \neq 0, m} (J_{0m}^x J_{mn}^x J_{n0}^x + J_{0m}^y J_{mn}^y J_{n0}^y + J_{0m}^z J_{mn}^z J_{n0}^z) - 3 \sum_{m \neq 0} J_{0m}^x J_{0m}^y J_{0m}^z \right\}. \quad (5)$$

The first summation in eq. 5 is always zero for a lattice not containing triangles while the second sum is zero for XY interactions. So, c_3 vanishes on a square lattice with XY interaction^{††} as can also be seen from eq. 1. In case of the more elaborate model applicable to $\text{CoBr}_2 \cdot 6\text{H}_2\text{O}$, as discussed in chapter I, eqs. 4 and 5 read ($S = \frac{1}{2}$):

$$c_2 = \frac{1}{2} \left\{ (J_1^x)^2 + (J_1^y)^2 + (J_1^z)^2 \right\} + \frac{1}{4} \left\{ (J_2^x)^2 + (J_2^y)^2 + (J_2^z)^2 \right\} \quad (6)$$

$$c_3 = \frac{3}{4} \left[2 \left\{ (J_1^x)^2 J_2^x + (J_1^y)^2 J_2^y + (J_1^z)^2 J_2^z \right\} - 2 J_1^x J_1^y J_1^z - J_2^x J_2^y J_2^z \right]. \quad (7)$$

To estimate the next nearest neighbour interaction J_2^{\ddagger} we assume that

$$J_2^{\ddagger} = \rho J_1^{\ddagger}, \quad (8)$$

a relation that will hold exactly if dipolar interactions are negli-

††

In contrast with the coefficient c_3 , the coefficient b_3^α of T^{-3} in the HTE of the reduced susceptibility $\chi_\alpha / (N g_\alpha^2 \mu_B^2)$ ($\alpha = x, y, z$) does not vanish on a square lattice with XY interaction. This follows from permutation of axes and specialization of the general expression for b_3^z resulting from the Hamiltonian eq. 3 i.e.

$$\begin{aligned}
 b_3^z = & \frac{2 S^2 (S+1)^2}{27 k^2} \left[\frac{(2S-1)(2S+3)}{5} \sum_{m \neq 0} (J_{m0}^z)^2 \right. \\
 & - \frac{2S^2 + 2S + 1}{5} \sum_{m \neq 0} \left\{ (J_{m0}^x)^2 + (J_{m0}^y)^2 \right\} - \frac{1}{2} \sum_{m \neq 0} J_{m0}^x J_{m0}^y \\
 & \left. + 2S(S+1) \sum_{m \neq 0} \sum_{n \neq 0, m} J_{m0}^z J_{mn}^z \right].
 \end{aligned}$$

Thus, b_3^α is not very suitable to estimate deviations from the XY square lattice.

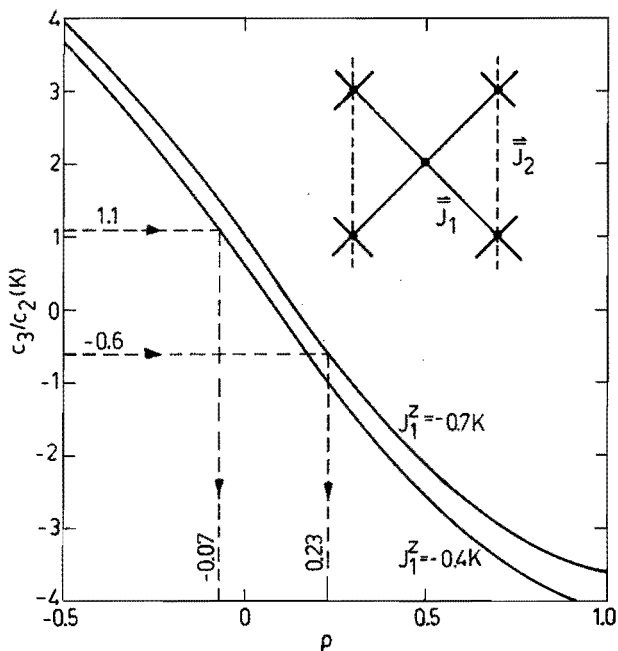


Figure IV-6.

The quotient c_3/c_2 , calculated from equations (6) and (7) with $J_1^x = J_1^y = -2.4$ K and $J_2^z = \rho J_1^z$, as a function of ρ for two different values of J_1^z . For a further explanation the reader is referred to the text.

gible and if the exchange is isotropic in the full spin. We calculated c_3/c_2 as a function of ρ with $J_1^x = J_1^y = J_{xy} = -2.4$ K and -0.7 K $\leq J_1^z = J_2^z \leq -0.4$ K (see table III-3 for the values of J_{xy} and J_z). Comparison of this calculated quotient with the experimental range -0.6 K $< c_3/c_2 < 1.1$ K yields $-0.1 \leq \rho \leq 0.25$ as is shown in fig. IV-6. This implies that -0.6 K $\leq J_2^{x,y} \leq 0.25$ K. It should be pointed out that the reliability of this estimate is endangered if the lattice specific heat does not behave like T^3 , since this would mean a possible cancellation of systematic errors in the description of the lattice and the magnetic contribution.

Discussion of the parameter values in connection with the results obtained by other techniques will be postponed till chapter V.

4.4 References.

- 1) H. Forstat, G. Taylor and R.D. Spence,
Phys. Rev. 116, 897 (1959).
- 2) J. Skalyo and S.A. Friedberg,
Phys. Rev. 13, 133 (1964).
- 3) L. Onsager,
Phys. Rev. 65, 117 (1944).
- 4) D.J. Wallace in
Phase Transitions and Critical Phenomena, Vol. VI, p. 352,
(C. Domb and M.S. Green, Eds.), Academic Press,
New York, 1976.
- 5) G.A. Baker Jr., B.G. Nickel and D.I. Meiron,
Phys. Rev. B17, 1365 (1978).
- 6) D.D. Betts, C.J. Elliott and R.V. Ditzian,
Can. J. Phys. 49, 1327 (1971).
- 7) D.D. Betts, J.T. Tsai and C.J. Elliott,
Proceedings of the International Conference on Magnetism, (1974),
Vol. IV, p. 279.
- 8) J. Rogiers, T. Lookman and D.D. Betts,
Can. J. Phys. 56, 409 (1978).
- 9) L.J. de Jongh, D.D. Betts and D.J. Austen,
Solid State Comm. 15, 1711 (1974).
- 10) T. de Neef and J.P.A.M. Hijmans,
J. Phys. A9, 105 (1976).

CHAPTER V

DISCUSSION ON $\text{CoBr}_2 \cdot 6\text{H}_2\text{O}$.

5.1 Introduction.

In the foregoing chapters we presented the results of various experiments on $\text{CoBr}_2 \cdot 6\text{H}_2\text{O}$. The data were analyzed with several interaction models all of which assumed a spatial 2-dimensional array (square or more complex) with a predominant XY-character ($|J_n^x| \approx |J_n^y| \gg |J_n^z|$) of the interaction. In the case of the high-temperature susceptibility the interaction model was supplemented with a crystal-field effect, while in the analysis of the specific heat measurements the lattice contribution had to be estimated. The use of a specific model is determined by several factors. Among those are the availability of theoretical expressions, the accuracy of the measurements and the sensitivity of the physical quantity under consideration for the parameters occurring in a particular choice of model. In this case this leads to the situation that, in principle, non of the quantitative results can be compared directly because they were obtained with slightly different models. In order to obtain a more complete picture we will present in this chapter some additional data and methods of interpretation.

5.2 Molecular Field approximations.

First we will establish a relation between the microscopic exchange tensors in $\text{CoBr}_2 \cdot 6\text{H}_2\text{O}$ and the parameters dominating the Molecular Field (MF) description^{1,2)} of a two-sublattice antiferromagnet with a relatively high anisotropy.

This relation will provide the link between the results of high-temperature theories, formulated in terms of microscopic parameters, and the results of experiments performed in the ordered state, for which usually only MF-descriptions are available.

Within the framework of MF-theory the energy density is written as

$$E = \vec{M}_+^T \vec{A} \vec{M}_- + \frac{1}{2} (\vec{M}_+^T \vec{I} \vec{M}_+ + \vec{M}_-^T \vec{I} \vec{M}_-), \quad (1)$$

where \vec{M}_+ and \vec{M}_- represent the modified magnetizations of the + and - sublattices, respectively, while the modified magnetizations are defined as

$$\vec{M}_\pm = 2 \frac{1}{g} \cdot (\vec{M}_\pm)_{\text{real}} . \quad (2)$$

On the other hand we have the microscopic Hamiltonian

$$H = -2 \sum_i \sum_{j<i} \vec{S}_i^T \cdot \vec{J}_{ij} \cdot \vec{S}_j = - \sum_i \vec{S}_i^T \cdot \sum_{j \neq i} \vec{J}_{ij} \cdot \vec{S}_j , \quad (3)$$

where the \vec{S}_i are the effective spin operators of the Co^{2+} ions. Because two-spin correlation functions are decoupled in the simple MF-approximation according to

$$\langle S_i^\alpha S_j^\beta \rangle = \langle S_i^\alpha \rangle \langle S_j^\beta \rangle \quad (\alpha, \beta = x, y, z, \quad i \neq j)$$

one obtains from eq. 3 the energy of spin i as

$$E_i = - \langle \vec{S}_i^T \rangle \cdot \sum_{j \neq i} \vec{J}_{ij} \cdot \langle \vec{S}_j \rangle . \quad (4)$$

In the absence of a magnetic field each spin in a two-sublattice antiferromagnet contributes the same amount to the energy and consequently the energy per mole is given by

$$E = N E_0 = - N \langle \vec{S}_0^T \rangle \cdot \sum_{j \neq 0} \vec{J}_{0j} \cdot \langle \vec{S}_j \rangle . \quad (5)$$

Taking into account the specific properties of $\text{CoBr}_2 \cdot 6\text{H}_2\text{O}$ we proceed as follows. From the magnetic space group $C_{2/m}^{2,3,4}$ it follows that each Co^{2+} ion interacts with four neighbours on the other sublattice (\vec{J}_1) and with two nearest neighbours on the same sublattice (\vec{J}_2). The reader is referred to chapter I for the labelling of the interactions as well as for their conjectured relative magnitudes from which it seems plausible to neglect the next nearest neighbour interaction \vec{J}_3 and the coupling between the ab layers in this context. Choosing \vec{S}_0 on the + sublattice, eq. 5 results in

$$E = - N \langle \vec{S}_+^T \rangle \cdot (4 \vec{J}_1 \cdot \langle \vec{S}_- \rangle + 2 \vec{J}_2 \cdot \langle \vec{S}_+ \rangle) . \quad (6)$$

The expectation values $\langle \vec{S}_{\pm} \rangle$ are related to the modified magnetizations \vec{M}_{\pm} (eq. 2) by

$$\vec{M}_{\pm} = 2 g^{-1} \left(\frac{N}{2} g \mu_B \langle \vec{S}_{\pm} \rangle \right) = N \mu_B \langle \vec{S}_{\pm} \rangle , \quad (7)$$

which yields, in combination with eq. 6,

$$E = - \vec{M}_{+}^T \left(\frac{4 J_1}{N \mu_B^2} \vec{M}_{-} + \frac{2 J_2}{N \mu_B^2} \vec{M}_{+} \right) . \quad (8)$$

Comparison of eqs. 1 and 8 reveals that

$$\vec{A} = - \frac{4 J_1}{N \mu_B^2} , \quad \vec{\Gamma} = - \frac{2 J_2}{N \mu_B^2} . \quad (9)$$

Because existing MF-theories for a compensated antiferromagnet assume that the principal axes of \vec{A} and $\vec{\Gamma}$ coincide, we have to make the same assumption for \vec{J}_1 and \vec{J}_2 in view of eq. 9. The labelling of the principal axes is fixed by the requirement that

$$-A_x + \Gamma_x < -A_y + \Gamma_y < -A_z + \Gamma_z . \quad (10)$$

From, essentially zero-temperature, energy considerations it follows that, with this choice, the spins order antiferromagnetically along the x-direction (preferred direction).

The z-axis (hard axis) is the least favourable direction for an antiferromagnetic ordering while the energy of a spin ordering along the y-axis (intermediate axis) is in between that of an ordering along x- or z-axis. It should be pointed out that we employed this labelling already in the interpretation of the high-temperature susceptibility data. (See fig. III-2 for the orientation of the x,y,z coordinate system with respect to the crystallographic axes a,b,c). Although we had to assume there $J_1^x = J_1^y$ (and $\vec{J}_2 = \vec{0}$), because otherwise HTE-s with sufficient terms are not known, it will be clear from eqs. 9 and 10 that the exchange component J_1^x has to be stronger than J_1^y . This conclusion remains valid if we suppose that $\vec{J}_2 = \rho \vec{J}_1$ provided that $\rho < 2$, which was confirmed in chapter IV ($-0.1 < \rho < 0.25$).

The fact that the high-temperature susceptibility χ_y is slightly larger than χ_x (see fig. III-3) is thus probably caused by a slightly stronger J_1^x and should not be explained with $g_y > g_x$ (Ch. III, $g_y = 4.82$, $g_x = 4.70$) which seems merely a consequence of the constraint $J_1^x = J_1^y$. (Therefore we will assume a mean value $g_x = g_y = 4.76$ in the following).

In view of the uncertainties concerning the XY-plane anisotropy, we performed AFMR experiments using the experimental set-up sketched in chapter II. Such experiments not only yield *direct* information on the XY-plane anisotropy but, in principle, also permit a rather accurate determination of $\frac{\hbar}{\Gamma}(J_2^z)$. The results at $T = 1.2$ K are shown in figure V-1, together with the data reported by Murray and Wessel⁵⁾, and will be analyzed using the theory developed by Date^{2,6)}. Because the expressions for the resonance frequencies are formulated most elegantly in terms of modified susceptibilities, i.e. $\chi = \left(\frac{2}{g}\right)^2 \chi_{\text{exp}}$, we will use modified quantities throughout the following. In order to obtain the XY-plane anisotropy we will first focus on the resonance frequency at $H = 0$, which is given by

$$\left(\frac{\omega}{\gamma}\right)^2 = \frac{2 M_0^2}{\chi_z} \left[(A_x - A_y) - (\Gamma_x - \Gamma_y) \right] = \frac{2 M_0^2}{\chi_z} \Delta_{xy} . \quad (11)$$

Here, γ is the gyromagnetic ratio of the free electron. The magnitude M_0 of the sublattice magnetization is found in MF-theory, at $T = 0$ K, from (eq. 7) $M_0 = \frac{1}{2} N \mu_B$. As can be seen from figure V-2, we may neglect the difference in the value of M_0 at $T = 1.2$ K and at $T = 0$ K. If we insert the experimental value $\left(\frac{\omega}{\gamma}\right)_0 = 14.3 \pm 0.2$ kOe together with the value of χ_z inferred from susceptibility measurements at $T = 1.2$ K (see table V-1), we find $\Delta_{xy} = 0.67$ mol/emu. Supposing that $\frac{\hbar}{J_2^z} = \rho \frac{\hbar}{J_1^z}$, this value of Δ_{xy} yields, in combination with eqs. 9 and 11,

$$\left(1 - \frac{1}{2} \rho\right) (J_1^x - J_1^y) = -0.063 \text{ K} ,$$

which amounts to only 2.5% of the mean value $J_1^x = J_1^y = -2.37$ K. Regardless of the precise value of ρ ($-0.1 < \rho < 0.25$) this implies a very small XY-anisotropy of $\frac{\hbar}{J_1^z}$.

Now we consider the field dependence of the resonances. The theoretical descriptions of the AFMR branches for $H//x$, with $H > H_c$, and for $H//y$ are

$$\left(\frac{\omega}{Y}\right)^2 = \left[1 - \frac{\chi_z^2}{4 M_0^2} \left(\frac{\omega}{Y}\right)_0^2 \right] \times \left[\frac{\chi_F^2}{\chi_y \chi_z} H_x^2 - \left(\frac{\omega}{Y}\right)_0^2 \right] \quad (12)$$

and

$$\left(\frac{\omega}{Y}\right)^2 = \frac{\chi_y^2}{\chi_F \chi_z} H_y^2 + \left(\frac{\omega}{Y}\right)_0^2, \quad (13)$$

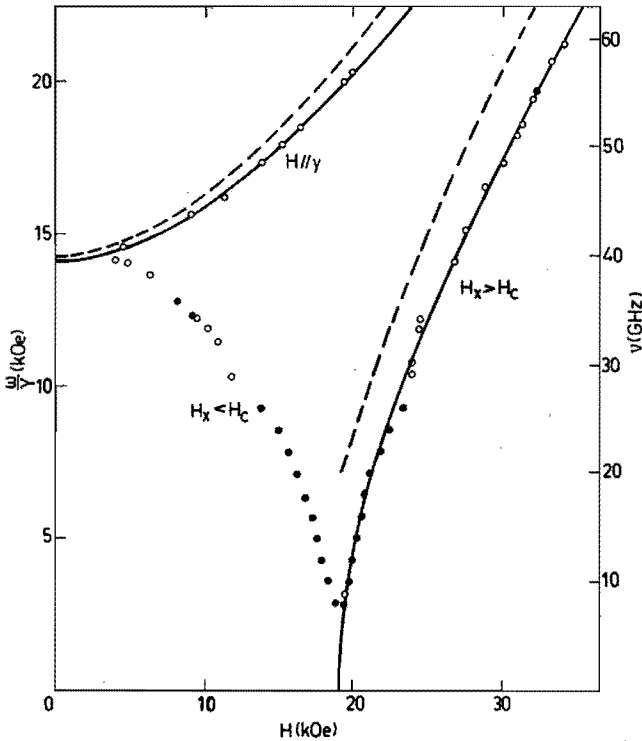


Figure V-1.

AFMR frequency versus modified field $H = \frac{g}{2} H_{exp}$. ($g_x = g_y = 4.76$) in $CoBr_2 \cdot 6H_2O$ at $T = 1.2$ K. Open data points are taken from reference 5. Fully drawn lines represent the result (eq. 14) of fits with a function of the type $\frac{\omega}{Y} = \sqrt{aH^2 + b}$ while the dashed curves describe the predictions (eq. 15) obtained from the susceptibilities at $T = 1.2$ K.

Table V-1.

Susceptibilities of $\text{CoBr}_2 \cdot 6\text{H}_2\text{O}$ at $T = 1.2 \text{ K}$ in units of 10^{-2} emu/mol . The column marked "experimental" contains the measured values after correction for van Vleck magnetism. The modified susceptibilities $\chi_{\text{mod}} = \left(\frac{2}{g}\right)^2 \chi_{\text{exp}}$ are calculated with $g_x = g_y = 4.76$ and $g_z = 2.02$.

	experimental	modified
$H_x < H_c$	$\chi_{//} = 2.9$	$\chi_{//} = 0.51$
$H_x > H_c$	$\chi_F = 19.5$	$\chi_F = 3.44$
$H // y$	$\chi_y = 18.8$	$\chi_y = 3.32$
$H // z$	$\chi_z = 5.23$	$\chi_z = 5.13$

respectively. Here, χ_F denotes the susceptibility in the spin-flop state where the spins are approximately antiferromagnetically aligned along the y-axis while the field is directed along the x-axis. This state occurs when H_x exceeds the critical field H_c . Fitting the data on these branches with the function $\frac{\omega}{Y} = \sqrt{aH^2 + b}$ yields

$$\left(\frac{\omega}{Y}\right)^2 = 0.569 H_x^2 - 207, \quad \left(\frac{\omega}{Y}\right)^2 = 0.531 H_y^2 + 199, \quad (14)$$

where $\frac{\omega}{Y}$ and H_α are measured in kOe. On the other hand we can calculate the coefficients a and b from eqs. 12 and 13 using essentially only experimentally determined quantities, i.e. $\left(\frac{\omega}{Y}\right)_0$ and the (modified) susceptibilities tabulated in table V-1. The fact that an experimental value of M_0 is lacking is of little importance here because the first factor in the righthand side of eq. 12 is almost unity (we find 0.982 with $M_0 = \frac{1}{2} N \mu_B$). The result is

$$\left(\frac{\omega}{Y}\right)^2 = 0.682 H_x^2 - 201, \quad \left(\frac{\omega}{Y}\right)^2 = 0.624 H_y^2 + 204. \quad (15)$$

Comparison of eqs. 14 and 15 or inspection of fig. V-1, in which both sets of equations are plotted, reveals an obvious discrepancy in the coefficients of H^2 ($0.682/0.569 = 1.20$, $0.624/0.531 = 1.18$). A possible cause for these deviations might be that the susceptibilities occurring

in the resonance conditions are tacitly assumed to equal their static values, thereby neglecting a possible frequency dependence. We did not try to evaluate this idea because there may also be complications of a quantum-mechanical nature, as we shall see further on.

Another kind of inconsistency can be shown as follows. The susceptibilities in the ordered state are given by MF theory as

$$\chi_{\alpha} = \frac{2}{A_x + A_{\alpha} - \Gamma_x + \Gamma_{\alpha}} \quad (\alpha = y, z) \quad (16)$$

$$\chi_F = \frac{2}{A_x + A_y + \Gamma_x - \Gamma_y}$$

We calculated these quantities from our high-temperature results for $\frac{z}{J_1}$ ($J_1^x = J_1^y = -2.37$ K, $J_1^z = -0.7$ K), with the aid of eq. 9 and with the assumption that $\frac{z}{J_2} = \rho \frac{z}{J_1} = 0.1 \frac{z}{J_1}$. It should be noted that g-values are not required to obtain the modified susceptibilities (eq. 16) in this way. Furthermore, the results for χ_y and χ_F are equal and independent of the actual value of ρ because axial symmetry in $\frac{z}{J_2}$ implies that $\Gamma_x = \Gamma_y$. The outcome of the calculation is

$$\chi_F = \chi_y = 3.96 \times 10^{-2} \text{ emu/mol}, \quad \chi_z = 6.28 \times 10^{-2} \text{ emu/mol} .$$

These values are, in the mean, 19% higher than those following from susceptibility measurements at $T = 1.2$ K (see table V-1). However, the ratio $\chi_F : \chi_y : \chi_z = 1 : 1 : 1.58$, found in the present calculation, matches rather well with the ratio $\chi_F : \chi_y : \chi_z = 1.04 : 1 : 1.55$ obtained from table V-1. The fact that the susceptibilities calculated in the MF-approach are systematically higher than the experimental values may be explained by the existence of a spin reduction, which has been observed to be rather important in this compound⁷⁾. Because spin-wave calculations on two-dimensional XY-like systems seem not yet available, we don't see a way to account accurately for quantum effects at this moment.

5.3 Spatial dimensionality.

So far, the interactions are assumed to act only between ions in the ab layers. This raises the question whether $\text{CoBr}_2 \cdot 6\text{H}_2\text{O}$ might be adequately

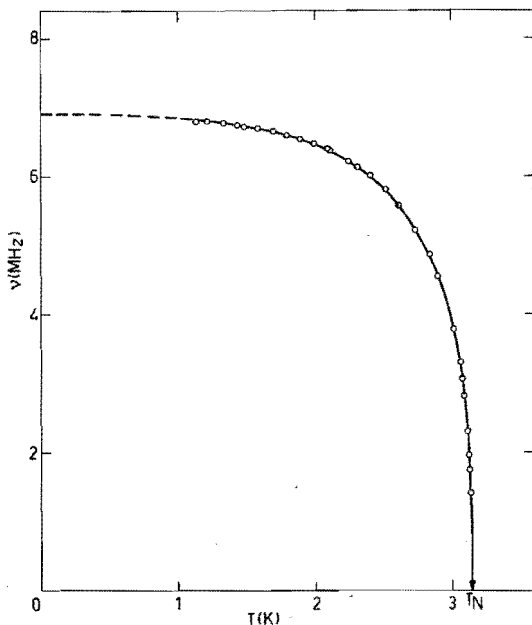


Figure V-2.

Temperature dependence of a proton resonance frequency in $\text{CoBr}_2 \cdot 6\text{H}_2\text{O}$. The internal field at a proton site is directly proportional to the magnitude of the sublattice magnetization.

described by a two-dimensional XY model. Theoretical calculations by Betts et al.^{8,9)} on several XY models reveal for the f.c.c. lattice and the triangular lattice a critical entropy of 0.52 R and 0.27 R respectively. The two-dimensional model however does not show any singularity in the specific heat. We are inclined to believe that this compound may be approximated by a square lattice rather than a triangular lattice as can be seen from the geometry of the interactions and the relative magnitude of \vec{J}_1 and \vec{J}_2 . For the Ising model it has been shown that the critical entropy mainly depends on the lattice dimensionality, while the dependence on the detailed lattice structure seems to be rather small^{10,11)}. Although calculations on the XY model are less extensive, the available evidence strongly suggests that the critical entropy will show the same tendency. The value 0.39 R inferred from our specific heat measurements (see chapter IV) therefore could indicate a

system with a behaviour in between that of the pure two- and three-dimensional case.

Additional information about the dimensionality may be obtained from the critical behaviour of the sublattice magnetization. Van der Lugt and Poulis¹²⁾ measured the sublattice magnetization of the isostructural $\text{CoCl}_2 \cdot 6\text{H}_2\text{O}$ by means of a proton NMR technique and from their data a critical exponent $\beta = 0.18$ was inferred¹³⁾ which would indicate a two-dimensional ordering at $T = T_N$. However, their experiments did not extend nearer to T_N than $(1-T/T_N) \approx 0.04$. As this still may be outside the critical region, we thought it worthwhile to investigate the behaviour of the sublattice magnetization of both $\text{CoCl}_2 \cdot 6\text{H}_2\text{O}$ and $\text{CoBr}_2 \cdot 6\text{H}_2\text{O}$ for $(1-T/T_N) < 0.04$. Since the results for both compounds are very similar, we will only present data on the bromine compound. Fig. V-3 shows a double logarithmic plot of a proton NMR frequency ν versus $(1-T/T_N)$. The critical exponent β is given by the slope of the drawn line, which corresponds to $\beta = 0.31 \pm 0.02$ in

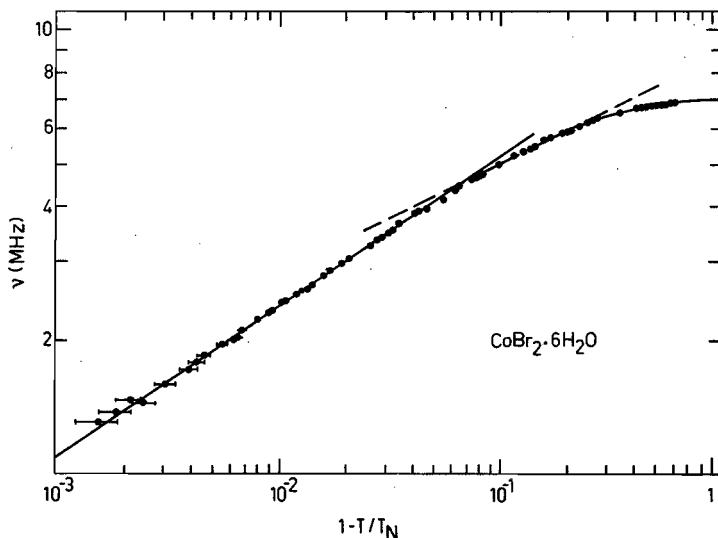


Figure V-3.

Plot of a proton NMR frequency ν versus $(1-T/T_N)$ for $\text{CoBr}_2 \cdot 6\text{H}_2\text{O}$. The slope of the drawn line corresponds to a critical exponent $\beta = 0.31 \pm 0.02$. The dashed line may be compared with earlier results on $\text{CoCl}_2 \cdot 6\text{H}_2\text{O}$ ¹²⁾.

the range $2 \times 10^{-3} < (1-T/T_N) < 0.06$. This value may be compared with the result $\beta = 0.326 \pm 0.05$ ¹⁴⁾ of recent neutron diffraction experiments on $\text{CoBr}_2 \cdot 6(0.52 \text{ H}_2\text{O}, 0.48 \text{ D}_2\text{O})$ in the temperature range $10^{-4} < (1-T/T_N) < 0.02$. Although these values are close to the prediction $\beta = 0.346$ for the three-dimensional XY model¹⁵⁾ they are even closer to the exponent $\beta = 0.325$ of the three-dimensional Ising model¹⁶⁾. Anyhow, the ordering phenomena at $T = T_N$ seem to be mainly three-dimensional in nature and therefore the conjectured smallness of the inter-layer interaction is not confirmed. The assumption is not rejected either, because even a small coupling between two-dimensional sub-systems might cause a three-dimensional critical behaviour.

5.4 References.

- 1) O.P. van Wier, T. van Peski-Tinbergen and C.J. Gorter, *Physica* 25, 116 (1959).
- 2) M. Date, *J. Phys. Soc. Japan* 16, 1337 (1961).
- 3) R.D. Spence, P. Middents, Z. El Saffar and R. Kleinberg, *J. Appl. Phys.* 35, 854 (1964).
- 4) R. Kleinberg, *J. Chem. Phys.* 53, 2660 (1970).
- 5) T.E. Murray and G.K. Wessel, *J. Phys. Soc. Japan* 24, 738 (1968).
- 6) M. Date and M. Motokawa, *J. Phys. Soc. Japan* 22, 165 (1967).
- 7) J.W. Metselaar, L.J. de Jongh and D. de Klerk, *Physica* 79 B, 53 (1975).
- 8) D.D. Betts, C.J. Elliott and R.V. Ditzian, *Can. J. Phys.* 49, 1327 (1971).
- 9) D.D. Betts, J.T. Tsai and C.J. Elliott, *Proceedings of the International Conference on Magnetism (1974)*, Vol. IV, p.279.
- 10) C. Domb, *Adv. Phys.* 9, 149, 245 (1960).
- 11) C. Domb and A.R. Miedema, *Prog. Low Temp. Phys.* 4, 296 (1964).
- 12) W. van der Lugt and N.J. Poulis, *Physica* 26, 917 (1960).
- 13) L.J. de Jongh and A.R. Miedema, *Adv. Phys.* 23, 1 (1974).
- 14) J.A.J. Basten, *Proc. of the Int. Symp. on Neutron Inelastic Scattering (IAEA, Vienna 1978)*, Vol. II, 247.
- 15) G.A. Baker Jr., B.G. Nickel and D.I. Meiron, *Phys. Rev. B* 17, 1365 (1978).
- 16) J.C. le Guillou and J. Zinn-Justin, *Phys. Rev. Letters* 39, 95 (1977).

CHAPTER VI

ISOTOPE EFFECTS.[†]

6.1 Introduction.

In view of the interest in the critical behaviour of 2d-XY systems, of which $\text{CoCl}_2 \cdot 6\text{H}_2\text{O}$ and $\text{CoBr}_2 \cdot 6\text{H}_2\text{O}$ seemed to be two of the very rare examples, and considering the fact that research in this field leans rather heavily on neutron diffraction experiments, it was desirable to deuterate these compounds in order to avoid the excessive incoherent background scattering caused by the hydrogen atoms. In almost all the cases which have been investigated experimentally, the deuteration of the water of hydration brings about only relatively insignificant changes in the crystallographic or magnetic properties¹⁾. In $\text{CoCl}_2 \cdot 6\text{H}_2\text{O}$ it was found²⁾, however, that already 3.5% deuteration caused anomalous effects which were attributed to a drastic change of the magnetic structure. It was concluded, that the original simple collinear two-sublattice system transforms to a four-sublattice system with hidden canting when the sample is deuterated^{5,6,7)}. Because such magnetic anomalies give rise to substantial complications in the analysis of neutron diffraction data, it seemed worthwhile to investigate whether or not $\text{CoBr}_2 \cdot 6\text{H}_2\text{O}$ could be deuterated to any practical extent without running into these difficulties. Anticipating the results, the rather unique isotope effect also found in $\text{CoBr}_2 \cdot 6\text{H}_2\text{O}$ deserved, in our opinion, appropriate attention by its own merits. When the work described in this chapter was in progress, a brief abstract on the effect of deuteration in $\text{CoBr}_2 \cdot 6\text{H}_2\text{O}$ with the emphasis on the change of the ordering temperature and deuterium resonance was published⁸⁾.

6.2 Experimental results.

Antiferromagnetic resonance. Antiferromagnetic resonance (AFMR) results on some partially deuterated $\text{CoBr}_2 \cdot 6[(1-f)\text{H}_2\text{O} \cdot f\text{D}_2\text{O}]$ crystals are shown

[†] Part of this chapter was published as:

J.P.A.M. Hijmans, W.J.M. de Jonge, P. van der Leeden and
M.J. Steenland, *Physica* 69, 76 (1973).

in figure VI-1. Referring to the coordinate system xyz (see figure III-2), the results can be described as follows. Up to $f = 0.55$ the preferred direction remains along the x-axis, while both ω at $H = 0$ and H_{crit} increase with increasing f (see also figure VI-2). For $f \geq 0.55$ the spectrum splits into two components, i.e. the type of resonance diagram originally observed with the field along the x-axis is now observed with the field at angles symmetrically around the x-axis in the xy plane. The angle with the x-axis increases with the

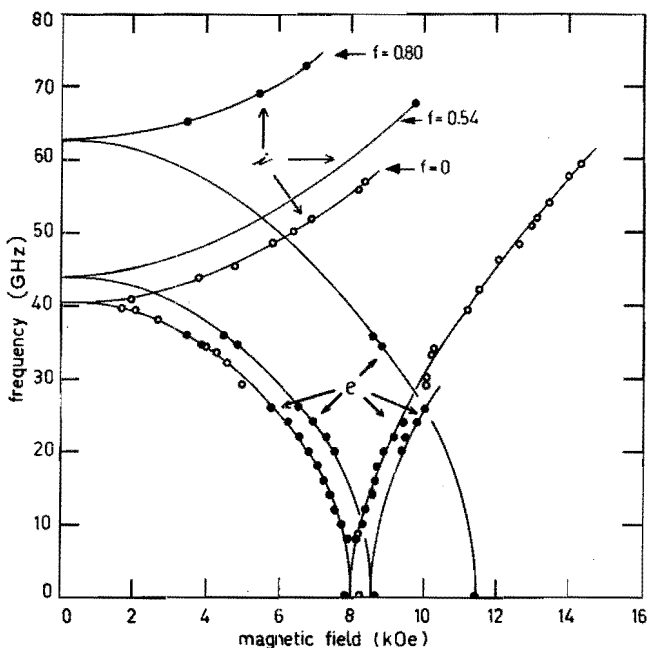


Figure VI-1.

Frequency-field diagram of the antiferromagnetic resonance in $\text{CoBr}_2 \cdot 6[(1-f)\text{H}_2\text{O} \cdot f\text{D}_2\text{O}]$ at 1.25 K for three values of the fraction D_2O . Open data points are taken from reference 9 ($f = 0$). Data on the branches marked (e) and (i) were collected with the field parallel to the easy and the intermediate axis respectively. The intermediate axis is perpendicular to the easy axis (preferred direction) and is situated in the xy plane. The orientation of the easy axis as a function of f is discussed in the text. Drawn curves are meant for visual aid only.

fraction f up to 32 degrees in the completely deuterated sample ($f = 1$). One of the most obvious results of these experiments is that they strongly suggest that above $f = 0.55$ the magnetic moments can be divided into two antiferromagnetic sets each turned away from the x -axis in the xy plane but in opposite directions. We will therefore refer to the directions of the magnetic field in which the above-mentioned resonances for $f > 0.55$ are observed as preferred directions, although it remains to be proven that the actual orientations of the sublattice magnetizations correspond to these directions.

The critical field. We studied the effect of deuteration on the AFMR-diagram more closely at frequencies of 1-10 MHz. The resonance phenomena we observed in this frequency range did not show any frequency dependence and consequently can be interpreted as essentially zero-frequency AFMR. With the external field applied exactly along the preferred direction(s) we assume to be tracing the critical field because it seems likely that a collective resonance mode at zero-frequency can only be caused by a magnetic phase transition. Figure VI-2 shows the magnitude and the direction of the critical field as a function of the deuterium fraction f . In the completely deuterated compound the critical field has increased by about 50% compared with the hydrate. Off-axis the resonance could only be detected in planes through the z -axis and the preferred directions. Within experimental accuracy the angle dependence of the resonant field in these planes can be described by $H_{\text{res}} \times \cos \theta = H_{\text{crit}}$, where θ is the angle of the field with the preferred direction. This angle dependence, which could be obtained experimentally for θ up to 45° , shows that the locus of resonant-field vectors is a straight line parallel to the z -axis and that the magnetic moments are restricted to the xy -plane in first approximation.

Proton resonance. In order to obtain information concerning the microscopic structure of $\text{CoBr}_2 \cdot 6[(1-f)\text{H}_2\text{O} \cdot f\text{D}_2\text{O}]$ we performed zero-field nuclear magnetic resonance (NMR) experiments on the hydrogen nuclei of the H_2O molecules. The results are shown in figure VI-3. For deuterium fractions $f < 0.55$ the situation is essentially the same as in $\text{CoBr}_2 \cdot 6\text{H}_2\text{O}$. The spectrum consists of four absorption lines originating from the four inequivalent proton positions, which exist in the crys-

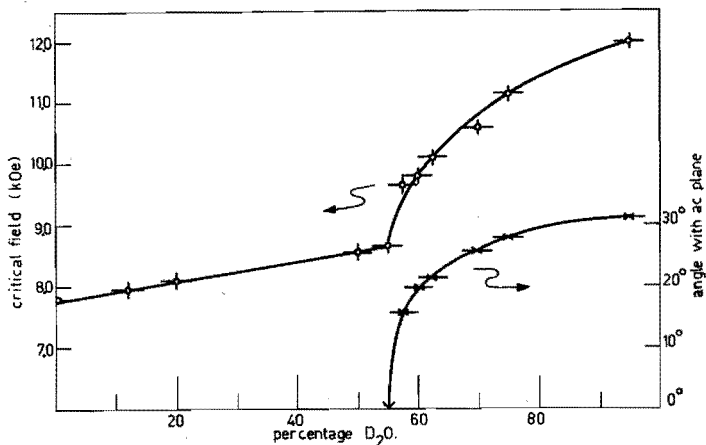


Figure VI-2.

Critical field parameters in $\text{CoBr}_2 \cdot 6[(1-f)\text{H}_2\text{O} \cdot f\text{D}_2\text{O}]$ at 1.15 K as a function of the deuterium fraction f .

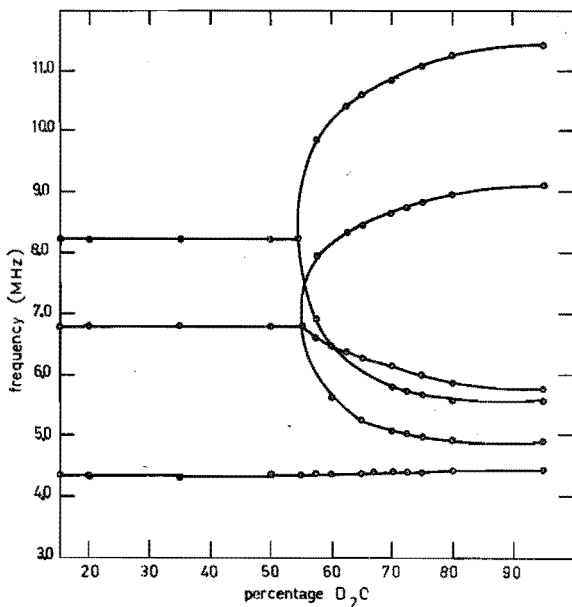


Figure VI-3.

Proton frequencies in $\text{CoBr}_2 \cdot 6[(1-f)\text{H}_2\text{O} \cdot f\text{D}_2\text{O}]$ at 1.15 K versus the deuterium fraction f . It should be noticed that for $f < 0.55$ two resonances accidentally coincide at a frequency of 6.8 MHz.

tallographic structure^{3,4}). Two of the protons occupy a general position and belong to the H₂O molecules incorporated in the CoBr₂O₄ clusters. The other two protons are situated at special positions in a mirror plane and belong to the H₂O molecules situated between successive layers consisting of CoBr₂O₄ clusters. For $f \geq 0.55$ the number of zero-field resonances changes from 4 to 6. Only those resonances double which arise from protons originally situated at a general position. The absorption lines at 4.4 and 6.8 MHz arising from the H₂O molecule originally situated in the mirror plane just change their frequency but do not double. These results show that above $f = 0.55$ the magnetic unit cell contains more inequivalent protons than can be accounted for by the original crystallographic structure. The conclusion that the crystallographic structure has changed is inevitable.

Bromine nuclear resonance. Our aim will be to determine the parameters which characterize the electric quadrupole interaction of a Br nucleus with its surroundings in CoBr₂·6D₂O and compare them with the corresponding parameters for CoBr₂·6H₂O in order to get some qualitative arguments about the structural change which apparently has taken place. Secondly, we want to obtain information about the direction of the individual magnetic moments from the direction of the hyperfine field at the bromine nucleus. The analysis of the bromine resonances in CoBr₂·6H₂O has been published by Rama Rao et al.¹⁰.

In the ordered state eight absorptions could be detected in CoBr₂·6D₂O which could be assigned to transitions of the ⁷⁹Br and ⁸¹Br nuclei (nuclear spin quantum number $I = 3/2$ for both isotopes). The frequencies are tabulated in table VI-1 and the temperature dependence is shown in figure VI-4. In the ordered state the bromine nuclei are subjected simultaneously to a Zeeman interaction and a quadrupole interaction. The Zeeman interaction of a nuclear spin \vec{I} with a magnetic field \vec{B} is given by

$$H_Z = - \gamma_N \hbar \vec{I} \cdot \vec{B} , \quad (1)$$

where γ_N is the gyromagnetic ratio of the nucleus under consideration. The interaction of the electric quadrupole moment Q ($I \geq 1$) with the electric field gradient (EFG) tensor $\vec{\nabla} \vec{E}$ can be written as

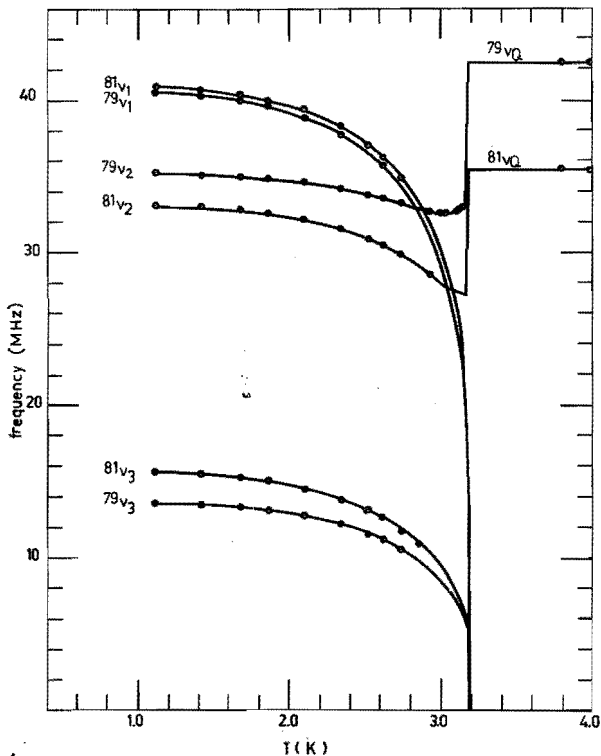


Figure VI-4.

Temperature dependence of the bromine nuclear resonance lines in $\text{CoBr}_2 \cdot 6\text{D}_2\text{O}$. The drawn curves are calculated using the parameters tabulated in Table VI-1 and the temperature dependence of a proton resonance frequency. The latter is assumed to be directly proportional to the Zeeman frequency ν_Z .

$$H_Q = \frac{e^2 q Q}{4I(2I-1)} \left[3I_Z^2 - I(I+1) + \frac{1}{2} \eta (I_+^2 + I_-^2) \right]. \quad (2)$$

Here the axes XYZ refer to the principal axes of $\vec{\nabla} \vec{E}$ which has the eigenvalues $-V_{XX}$, $-V_{YY}$ and $-V_{ZZ}$ respectively. The labelling of the axes is fixed by the requirement

$$|V_{XX}| \leq |V_{YY}| \leq |V_{ZZ}|. \quad (3)$$

Because the EFG tensor has vanishing trace, the eigenvalues of this

tensor are not independent and therefore a description in terms of the asymmetry parameter

$$\eta = (v_{XX} - v_{YY})/v_{ZZ} \quad (4)$$

and $q = v_{ZZ}/e$ is appropriate. The orientation of the field \vec{B} with respect to XYZ is specified by the polar and azimuthal angles θ and ϕ while the magnitude of the field is expressed in frequency units as

$$v_Z = \frac{\gamma_N}{2\pi} B. \quad (5)$$

The resonance frequency in the paramagnetic state in the absence of a magnetic field, known as the pure quadrupole resonance frequency v_Q , follows from

$$v_Q = \frac{3e^2qQ}{2I(2I-1)h} \sqrt{1 + \frac{1}{3} \eta^2}. \quad (6)$$

The general procedure to interpret the transition frequencies in terms of the Hamiltonian $H = H_Z + H_Q$, including the selection of the sets arising from ^{79}Br and ^{81}Br , as well as the labelling of the transitions v_1 , v_2 and v_3 between successive levels within a set, is outlined in a number of papers^{10,11)} and will not be repeated here. In this particular case, the existence of sumrelations (see table VI-1) simplifies the selection procedure considerably. The resulting parameters are tabulated in table VI-1.

The direction of the internal field at the bromine nucleus in the frame of the crystal axes was determined experimentally in the usual way through the linear combination of the gradients¹²⁾ of the transition frequencies v_1 , v_2 and v_3 :

$$\vec{v}_B = \frac{1}{10} \left(\frac{2\pi}{\gamma_N} \right)^2 \left[\left(\frac{3}{2} v_1 + v_2 + \frac{1}{2} v_3 \right) \vec{v}_B v_1 + (v_1 + 2 v_2 + v_3) \vec{v}_B v_2 + \left(\frac{1}{2} v_1 + v_2 + \frac{3}{2} v_3 \right) \vec{v}_B v_3 \right], \quad (7)$$

where $\vec{v}_B = \left(\frac{\partial}{\partial B_x}, \frac{\partial}{\partial B_y}, \frac{\partial}{\partial B_z} \right)$.

The gradient was determined experimentally by splitting the absorp-

Table VI-1.

Labelling of the frequencies and the interaction parameters for the bromine nuclei in $\text{CoBr}_2 \cdot 8\text{D}_2\text{O}$.

Nucleus	a) ν_i (MHz)	Label	ν_Q (MHz)	ν_Z (MHz)	θ	$\eta \cos 2\phi$
^{79}Br	13.56	ν_3		24.45	$79^\circ 30'$	0.01
	35.23	ν_2	$42.42^{\text{b)}$			
	40.51	ν_1	$42.47^{\text{c)}$			
	48.79	$\nu_2 + \nu_3$				
^{81}Br	15.57	ν_3		26.36	$79^\circ 30'$	0.01
	33.13	ν_2	$35.44^{\text{b)}$			
	40.95	ν_1	$35.48^{\text{c)}$			
	48.69	$\nu_2 + \nu_3$				

a) Measured at $T = 1.12$ K.

b) Experimental value at $T = 4.2$ K.

c) Calculated from ν_1 , ν_2 and ν_3 .

tion line by an external magnetic field of approximately 500 Gauss. The measured gradients (see also table VI-2) and the resultant field \vec{B} are shown in stereographic projection in figure VI-5. In this figure we also plotted the principal Z-axis (V_{ZZ}) of the electric field gradient as measured by splitting experiments of the pure quadrupole bromine lines in the paramagnetic state at $T = 4.2$ K. The angle θ between V_{ZZ} and B , as found from these splitting experiments, agrees very well with the θ value calculated from the spectrum ν_1 , ν_2 and ν_3 in the antiferromagnetic state.

The internal field at a bromine nucleus in the antiferromagnetic state is a summation of the hyperfine interaction with the Co^{2+} ion in the cluster and a dipole sum to account for the localized moments. Subtracting this last (in general small) contribution, the remaining hyperfine field can be written as

$$\vec{B}_{\text{hf}} = -(\gamma_N \hbar)^{-1} \vec{A} \cdot \langle \vec{S} \rangle, \quad (8)$$

where $\langle \vec{S} \rangle$ is the expectation value of the spin of the magnetic ion.

Table VI-2.

Magnitude and orientation of the gradients of the ^{79}Br and ^{81}Br lines in $\text{CoBr}_2 \cdot 6\text{D}_2\text{O}$ at $T = 1.12$ K. The angles α , β and γ are measured with respect to the orthogonal coordinate system a , b , c^* .

Nucleus	Label	$\frac{2\pi}{\gamma_N} \vec{V}_B \nu_i $	α	β	γ
^{79}Br	ν_1	1.274	100°	57°	35°
	ν_2	1.472	42.5°	72°	53°
	ν_3	2.536	172°	90°	98°
^{81}Br	ν_1	1.150	100°	56°	36°
	ν_2	1.199	57°	64°	44°
	ν_3	2.003	174°	84°	91°

Preliminary experiments on isostructural $\text{CoCl}_2 \cdot 6\text{H}_2\text{O}$ gave as results in the paramagnetic state $A_{a^*} = 5.16 \times 10^{-4} \text{ cm}^{-1}$, $A_b = 4.98 \times 10^{-4} \text{ cm}^{-1}$ and $A_c = 4.70 \times 10^{-4} \text{ cm}^{-1}$. The qualitative conclusion that the \vec{A} tensor in $\text{CoBr}_2 \cdot 6\text{H}_2\text{O}$ is also largely isotropic will probably be justified. This means that the direction of the hyperfine field at the bromine nucleus closely reflects the spin direction on the central ion. From figure VI-5 we see that the field at the bromine nucleus is shifted from the original direction in the ac plane towards the +b and -b axis by 33° , thus maintaining an apparent mirror symmetry with respect to the ac plane. These directions coincide within experimental accuracy with the directions in which the critical fields can be observed. This leads to the conclusion that *the magnetic structure can be described as two apparently independent systems with effectively no interaction.*

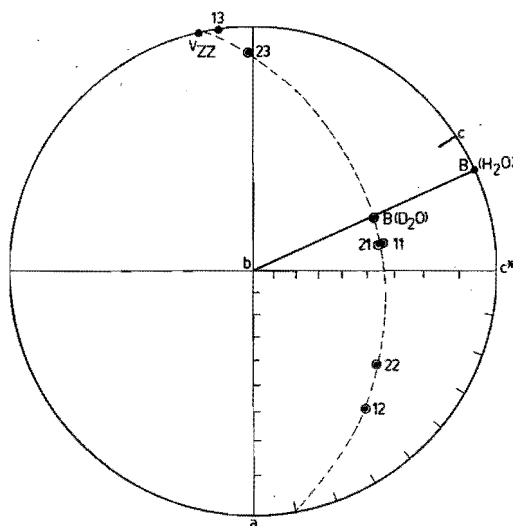


Figure VI-5.

Stereographic projection of the gradients $\vec{\nabla}_B \nu_{1i}$ and $\vec{\nabla}_B \nu_{2i}$ for respectively ^{79}Br and ^{81}Br nuclei in $\text{CoBr}_2 \cdot 6\text{D}_2\text{O}$ at $T = 1.12 \text{ K}$. Also shown are the resultant internal field \vec{B} and the experimental Z-axis V_{ZZ} of the electric field gradient tensor. The gradients, the internal field and V_{ZZ} are almost coplanar as a result of the very small value of the asymmetry parameter η .

A further conclusion concerns the crystallographic structure of the hydrated and the deuterated compound which, as we showed before, must be different. A comparison (see table VI-3) between the pure quadrupole resonance frequencies in the paramagnetic state of the two compounds shows that they differ only by 0.5⁰/00. Furthermore, the asymmetry parameters $\eta \cos 2\Phi$ differ only 0.01 and the directions of the principal Z-axes of the electric field gradients coincide within the experimental accuracy. Because all these parameters are very sensitive to structural changes we may conclude that in a first approximation neither the symmetry of the clusters in $\text{CoBr}_2 \cdot 6\text{D}_2\text{O}$ nor their orientation and spatial distribution have changed significantly compared with the hydrated compound.

Table VI-3.

Comparison of the internal field \vec{B} and the quadrupole interaction parameters for a ^{79}Br nucleus in $\text{CoBr}_2 \cdot 6\text{D}_2\text{O}$ and $\text{CoBr}_2 \cdot 6\text{H}_2\text{O}^{10}$.

The angles α , β and γ are the angles of \vec{B} with respect to the orthogonal coordinate system a , b , c^* .

	$ \vec{B} $ (kOe)	α	β	γ	ν_Q (MHz)	$\eta \cos 2\Phi$
$\text{CoBr}_2 \cdot 6\text{D}_2\text{O}$	22.92	110 ⁰	57 ⁰	40 ⁰	42.42	0.01
$\text{CoBr}_2 \cdot 6\text{H}_2\text{O}$	22.23	115 ⁰	90 ⁰	25 ⁰	42.40	0.02

6.3 Discussion.

The difference in magnetic structure between $\text{CoBr}_2 \cdot 6\text{H}_2\text{O}$ and $\text{CoBr}_2 \cdot 6\text{D}_2\text{O}$ cannot be explained without assuming a different crystallographic structure. The 2/m site symmetry of the Co^{2+} ion in

the hydrated compound allows only orientations of the magnetic moments parallel to the twofold b-axis (y-axis) or perpendicular to it. The canted cross-structure in the xy-plane, as we found it, is strictly forbidden in all the magnetic space groups belonging to the Opechowski¹³⁾ family of C 2/m. The direct evidence for such a structure difference between the two compounds is given by the proton resonance results reported here. Although this leads to a different group theoretical description of the crystal structure, bromine nuclear resonance showed that the geometry of the clusters remains almost unaffected. Probably we are dealing with some slight rearrangements.

If we want to select a crystallographic and a magnetic space group which are consistent with the experimental data so far, we have to fulfil the following conditions set by the experimental data:

1. The twofold rotation axis *and* the mirror plane at the Co^{2+} ion must vanish.
2. The inversion center at the Co site must remain because otherwise the bromine nuclei in one cluster would become inequivalent.
3. Equivalent nuclear sites, originally at a general crystallographic position, must become inequivalent in the new structure as can be concluded from the doubling of the proton absorption lines.

In an earlier interpretation of the data¹⁴⁾ these conditions were supplemented as follows:

4. The crystallographic space group must admit in one of its magnetic groups the aspect group 2/m as shown by the symmetry of the local fields at proton and bromine sites.
5. Assume that the crystallographic space group of $\text{CoBr}_2 \cdot 6\text{D}_2\text{O}$ will be a subgroup of C 2/m.

Condition 3 requires that one out of two possibilities applies. Either the unit cell becomes twice as large, or one of the generating symmetry elements in the space group C 2/m disappears completely. In view of the fact that successive face centered ab layers are

separated in the c direction by water molecules which apparently have a large influence on the structural change, the conjecture was made that the c-axis becomes twice as large. This would not be a unique case. It had been reported to occur for instance in $\text{Cu}(\text{COOH})_2 \cdot 4\text{H}_2\text{O}^{15}$ and $\text{NiCl}_2 \cdot 2\text{H}_2\text{O}^{16}$.

With this choice the construction of the new space group is easily completed. Because the new unit cell now contains 8 bromine nuclei which must be equivalent, the general position must be eight-fold. Within the assembly of subgroups of C 2/m this leaves only C 2/c and C 2/m. If it should be C 2/m it would require a general rearrangement of the symmetry elements in the unit cell according to condition 1 which is not in agreement with assumption 5. However, the space group C 2/c with $a = 11.0 \text{ \AA}$, $b = 7.2 \text{ \AA}$, $c = 13.8 \text{ \AA}$ and $\beta = 124^\circ$ qualitatively meets all the conditions set above. This change of space group is schematically depicted in figure VI-6.

According to the experiments the magnetic structure can be described as a cross structure consisting of two simple antiferromagnetic sets, canted with respect to each other and with a vanishingly small mutual interaction. Because the interaction between moments in neighbouring ab layers in the original structure can be considered as relatively weak, it seems reasonable to assume that the moments situated in one ab layer belong to one antiferromagnetic set canted with respect to the moments in neighbouring layers. Taking into account the original magnetic space group of $\text{CoBr}_2 \cdot 6\text{H}_2\text{O}$ and condition 5 one arrives at the magnetic space group $C_p 2/c$ with a magnetic array as sketched in figure VI-7.

To verify this proposed magnetic structure, neutron diffraction experiments were performed by Basten and Bongaarts¹⁷⁾. Their results did not confirm our proposal and can briefly be summarized as follows. The crystallographic structure of $\text{CoBr}_2 \cdot 6\text{D}_2\text{O}$ changes, at some temperature between 300 K and 4.2 K, from a high temperature C 2/m symmetry to a triclinic $P\bar{1}$ symmetry. Only small distortions of the monoclinic arrangements are involved in this phase transition. For instance, the cell parameters for C 2/m ($T = 300 \text{ K}$) are $a = 11.01 \text{ \AA}$, $b = 7.17 \text{ \AA}$, $c = 6.91 \text{ \AA}$ and $\beta = 124.8^\circ$ while for $P\bar{1}$ ($T = 4.2 \text{ K}$) the parameters are $a = 10.98 \text{ \AA}$, $b = 7.13 \text{ \AA}$, $c = 6.85 \text{ \AA}$, $\alpha = 89.4^\circ$, $\beta = 124.9^\circ$ and $\gamma = 89.8^\circ$. Besides a lowering of the symmetry, quite a different ef-

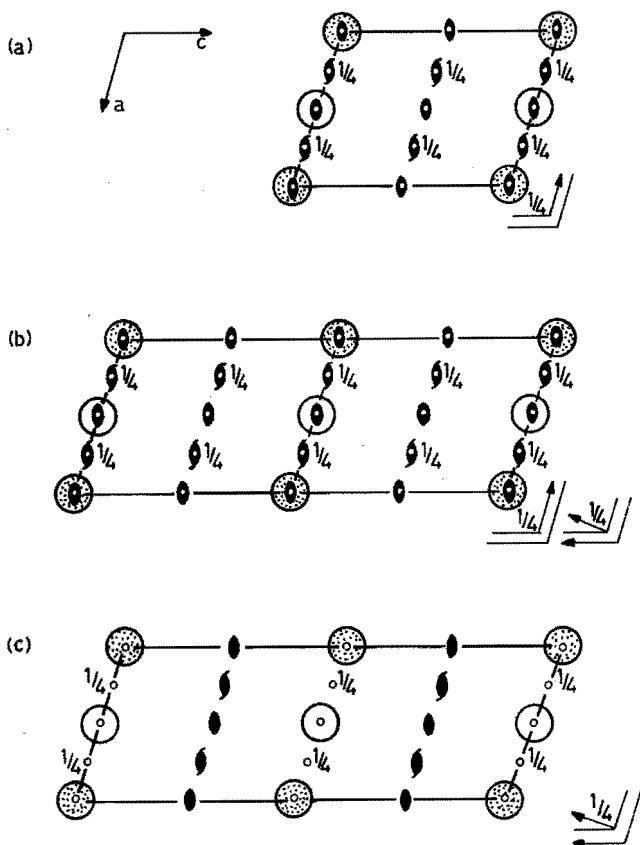


Figure VI-6.

Illustration of the change of space group in $\text{CoBr}_2 \cdot 6[(1-f)\text{H}_2\text{O} \cdot f\text{D}_2\text{O}]$ as suggested by the experimental resonance results.

Cobalt atoms are represented by shaded circles at the $b = 0$ level and by open circles at the level $b = \frac{1}{2}$. The symbolic representation of symmetry operations is according to the international notation¹⁸⁾.

(a) Symmetry elements of the space group $C 2/m$.

(b) The same set of symmetry operations as under (a) but with a doubled cell. Note the extra glide planes introduced by the doubling of the a -axis.

(c) Symmetry elements of the space group $C 2/c$. This group results from the situation described under (b) by omission of the two-fold rotation axis and the mirror plane at the cobalt position.

fect occurs at the phase transition: *the crystal breaks up in domains which have orientations related to each other by reflection symmetry around the ac^* plane*. Finally, neutron diffraction reveals that below the Néel temperature $\text{CoBr}_2 \cdot 6\text{D}_2\text{O}$ is a simple two-sublattice antiferromagnet. Compared with $\text{CoBr}_2 \cdot 6\text{H}_2\text{O}$, the only essential change in the magnetic structure is a rotation of the moments over an angle of $45^\circ \pm 15^\circ$ away from the ac plane (see figure VI-7).

Now let us re-examine the conclusions and conjectures obtained from the resonance experiments in the light of the neutron diffraction results:

a) Some of the conclusions were formulated as conditions for the new space group earlier in this paragraph. Conditions 1-3 are completely confirmed by the diffraction results, but conditions 4 and 5 turn out to be incorrect. The $2/m$ symmetry exhibited by the local fields at the proton and bromine sites in any sample of $\text{CoBr}_2 \cdot 6\text{D}_2\text{O}$ should not be identified with the symmetry of the unit cell but must be attributed to the existence of crystallographic domains.

b) The existence of these domains on a macroscopic scale is also consistent with our conclusion in section 6.2 that the system behaves as a combination of two simple antiferromagnetic systems with effectively no interaction; the two systems turn out to be completely independent indeed!

c) From the pure quadrupole Br resonance the positional changes of the ions in the $[\text{CoBr}_2\text{O}_4]$ -clusters were conjectured to be small. The neutron diffraction experiment confirms this conjecture.

d) The angle of the magnetic moment $\vec{\mu}$ with the ac plane is found by neutron diffraction as $45^\circ \pm 15^\circ$. In view of the relatively large error involved in this determination and the excellent agreement between the orientation found from the critical field direction and \vec{B}_{hf} as reported in this chapter it seems to us that the latter determinations are the more reliable. Therefore we quote that the moments in the deuterated sample are tilted towards the b -axis by an angle of $33^\circ \pm 2^\circ$ compared with the original direction close to the c -axis in $\text{CoBr}_2 \cdot 6\text{H}_2\text{O}$.

Concluding we may state that, although $\text{CoBr}_2 \cdot 6[(1-f)\text{H}_2\text{O} \cdot f\text{D}_2\text{O}]$ displays an anomalous behaviour when the percentage of deuteration

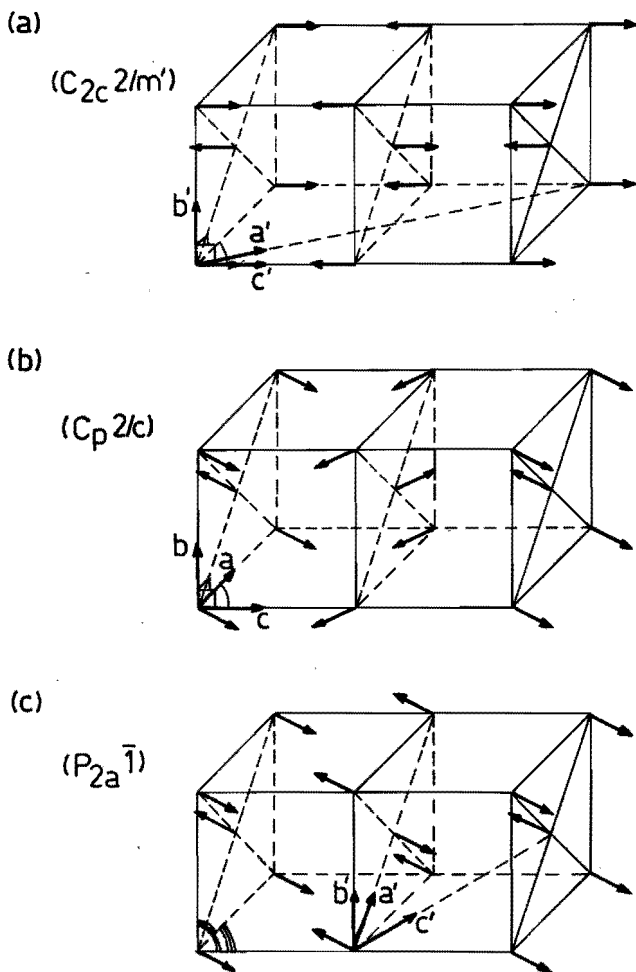


Figure VI-7.

(a) Magnetic structure of $\text{CoBr}_2 \cdot 6\text{H}_2\text{O}^{3,4}$.

(b) Monoclinic four-sublattice model proposed for $\text{CoBr}_2 \cdot 6\text{D}_2\text{O}$ in an earlier interpretation¹⁴⁾ of the resonance data.

(c) Triclinic two-sublattice model for $\text{CoBr}_2 \cdot 6\text{D}_2\text{O}$ inferred from neutron diffraction experiments¹⁷⁾.

The 8° angle between x - and c -axis has been omitted here for clearness sake. The Opechowski notations¹³⁾ are denoted with respect to the axes indicated in the corresponding figure.

exceeds 55%, the changes upon deuteration are relatively small. As far as the crystallographic structure is concerned, this assertion is supported by the minimum changes of the bromine quadrupole interaction parameters and, in greater detail, by the results obtained from neutron diffraction experiments ¹⁷⁾. Also the magnetic interactions appear not to be influenced appreciably. Comparison of the specific heat data for $\text{CoBr}_2 \cdot 6\text{H}_2\text{O}$ and $\text{CoBr}_2 \cdot 6\text{D}_2\text{O}$ (see table IV-2) reveals no significant change in dimensionality nor in the strength of the interactions. Only the 50% increase of the critical field and the large angle of rotation of the preferred direction do not seem to fit in this picture. However, these phenomena are delusive because they can easily be explained with additional anisotropies of a few percent (see chapter V) of the mean xy-plane interaction.

6.4 References

- 1) B.G. Turrell and C.L. Yue, *Can. J. Phys.* 47, 2575 (1969) and references there in.
- 2) H. Benoit, W. Ghidalia, J.P. Legrand and J.P. Renard, *J. Physique* 32, C1 - 1151 (1971).
- 3) R.D. Spence, P. Middents, Z. ElSaffar and R. Kleinberg, *J. Appl. Phys.* 35, 854 (1964).
- 4) R. Kleinberg, *J. Chem. Phys.* 53, 2660 (1970).
- 5) H. Benoit, J.P. Legrand and J.P. Renard, *C.R. Acad. Sc. Paris B* 264, 1556 (1967).
- 6) J.P. Legrand and J.P. Renard, *C.R. Acad. Sc. Paris B* 266, 1165 (1968).
- 7) B. Lecuyer and J.P. Renard, *C.R. Acad. Sc. Paris B* 269, 78 (1969).
- 8) J.P. Legrand and J.P. Renard in *Magnetic Resonance and Related Phenomena*, Proc. 17th Congress Ampere, edited by V. Hovi (North-Holland Publ. Co. 1973) p. 452.
- 9) T.E. Murray and G.K. Wessel, *J. Phys. Soc. Japan* 24, 738 (1968).
- 10) K.V.S. Rama Rao, W.J.M. de Jonge and C.H.W. Swüste, *Physica* 53, 621 (1971).
- 11) C.H.W. Swüste and K. Kopinga, *Physica* 60, 415 (1972).
- 12) R.D. Spence, J.A. Casey and V. Nagarajan, *Phys. Rev.* 181, 488 (1969).
- 13) W. Opechowski and R. Guccione in *Magnetism*, edited by Rado and Suhl (Academic Press Inc., N.Y. 1965), Vol. II A, chapter III.
- 14) J.P.A.M. Hijmans, W.J.M. de Jonge, P. van der Leeden and M.J. Steenland, *Physica* 69, 76 (1973).
- 15) G. Soda and T. Chiba, *J. Phys. Soc. Japan* 26, 249 (1969).
- 16) A.L.M. Bongaarts, B. van Laar, A.C. Botterman and W.J.M. de Jonge, *Phys. Letters* 41 A, 411 (1972).
- 17) J.A.J. Basten and A.L.M. Bongaarts, *Phys. Rev. B* 14, 2119 (1976).
- 18) *International Tables for X-ray Crystallography*, edited by N.F.M. Henry and K. Lonsdale (Kynoch Press, Birmingham, 1965), Vol. I.

SAMENVATTING

Het in dit proefschrift beschreven onderzoek had tot doel na te gaan in hoeverre het magnetisch gedrag van $\text{CoBr}_2 \cdot 6[(1-x)\text{H}_2\text{O} \cdot x\text{D}_2\text{O}]$ overeenkomt met dat van een twee-dimensionaal XY-model. Als uitgangspunt diende ondermeer het gegeven dat $\text{CoBr}_2 \cdot 6\text{H}_2\text{O}$ ($x = 0$) tot de weinige stoffen behoort die in redelijk goede benadering met een dergelijk model te beschrijven zijn. Om echter een betere indruk te krijgen van de afwijkingen ten opzichte van het ideale model was het noodzakelijk een aantal eigenschappen van deze stof zo gedetailleerd mogelijk te bepalen en te analyseren. De bestudering van de gedeutereerde verbindingen was in eerste instantie voornamelijk van belang voor een parallel lopend onderzoek door middel van neutron-diffractie, maar won aanmerkelijk in betekenis na het konstateren van een anomaal gedrag bij deuterium fracties x groter dan 0.55.

Na het inleidende hoofdstuk I, waarin, aan de hand van de kristallografische structuur, de globale magnetische eigenschappen van $\text{CoBr}_2 \cdot 6\text{H}_2\text{O}$ aannemelijk worden gemaakt, worden in hoofdstuk II de toegepaste experimentele technieken geschetst.

In hoofdstuk III wordt het gedrag van de susceptibiliteit van $\text{CoBr}_2 \cdot 6\text{H}_2\text{O}$ bij hoge temperaturen behandeld. Een kristalveld berekening, gekombineerd met hoge-temperatuur reeksontwikkelingen, leert dat de voornaamste afwijking van het XY-karakter bestaat uit een van nul verschillende wisselwerking tussen de Z-komponenten van de magnetische momenten. Tevens wordt aangetoond dat de aangeslagen toestanden van het Co^{2+} ion aanleiding geven tot een niet te verwaarlozen Van Vleck bijdrage in de susceptibiliteit.

Hoofdstuk IV heeft de temperatuurafhankelijkheid van de soortelijke warmte als onderwerp. Uit het verloop van deze grootheid bij temperaturen boven de ordeningstemperatuur volgt dat de op één na sterkste interactie in $\text{CoBr}_2 \cdot 6\text{H}_2\text{O}$ minstens een factor 4 zwakker is dan de voornaamste interactie. De interacties in $\text{CoBr}_2 \cdot 6\text{D}_2\text{O}$ blijken qua type en sterkte weinig van die in $\text{CoBr}_2 \cdot 6\text{H}_2\text{O}$ te verschillen.

De beschrijving van de geordende toestand van $\text{CoBr}_2 \cdot 6\text{H}_2\text{O}$ komt aan de orde in hoofdstuk V. Antiferromagnetische resonantie experimenten geven een exchange anisotropie in het XY-vlak van slechts enkele procenten aan. Een verdere konklusie, verkregen uit ondermeer het kritische gedrag van de subrooster magnetisatie, is dat het twee-dimen-

sionale karakter van $\text{CoBr}_2 \cdot 6\text{H}_2\text{O}$ niet tot uiting komt in de omgeving van de ordeningstemperatuur, maar slechts indirekt bewezen wordt door de goede overeenstemming tussen theorie en experiment bij hogere temperaturen.

Hoofdstuk VI, tenslotte, is gewijd aan het anomale gedrag van $\text{CoBr}_2 \cdot 6[(1-x)\text{H}_2\text{O} \cdot x\text{D}_2\text{O}]$ voor $x > 0.55$. De resultaten van diverse soorten resonantie experimenten tonen eenduidig aan dat er een kristallografische fase-overgang optreedt, die samengaat met een minieme vervorming van het rooster, en doen ten sterkste vermoeden dat de magnetische structuur uit een vier-subrooster systeem bestaat. Een onafhankelijk neutron-diffractie onderzoek wijst echter uit dat de structuur verandering gepaard gaat met een specifieke kristallografische domeinvorming die, samen met een normale twee-subrooster antiferromagnetische ordening, bij onderzoek met behulp van andere dan diffractie-technieken de indruk van een vier-subrooster systeem wekt.

DANKWOORD

De velen die, direkt of indirekt, hebben meegewerkt aan het totstandkomen van dit proefschrift wil ik hier danken. Mijn erkentelijkheid geldt, met excuses aan allen die onvermeld blijven, onder meer:

- alle leden en ex-leden van de groep Magnetisme voor een jarenlange prettige samenwerking,*
- Dr.ir. W.J.M. de Jonge bovendien voor zijn meer dan uitzonderlijke begeleiding,*
- Mej. M.C.K. Gruijters voor het bewerken van de tekeningen en*
- Mevr. M.T. Kossen-Schnabel en Mevr. A.M. Rijpkema-Hölscher voor het verzorgen van het typewerk.*

LEVENSBERICHT

27-08-1945 Geboren te Eindhoven

1964 Eindexamen HBS-B, Gemeentelijk Lyceum Eindhoven.

1964 - 1970 Studie aan de TH-Eindhoven, afdeling Technische Natuurkunde.
Afgestudeerd in de sectie Fysische Analyse Methoden onder
leiding van Prof.dr. P. van der Leeden.

1970 - 1978 Werkzaam in de groep Magnetisme van de TH-Eindhoven waar,
onder leiding van Dr.ir. W.J.M. de Jonge en
Prof.dr. P. van der Leeden, onder meer het promotie-
onderzoek werd verricht.

Sinds 1978 medewerker in de groep Fabrieks- en Apparatenbouw voor de
Procesindustrie, eveneens van de TH-Eindhoven, onder
leiding van Prof.ir. J.K. Nieuwenhuizen.

STELLINGEN

behorende bij het proefschrift van J.P.A.M. Hijmans

1. In verband met het onderzoek naar het optreden van een intermediaire magnetische fase in $\text{CoBr}_2 \cdot 6[0.52 \text{H}_2\text{O}, 0.48 \text{D}_2\text{O}]$ lijkt meting van het koppel, dat een kristal van deze stof in een homogeen magnetisch veld ondervindt, een aangewezen experiment.

J.A.J. Basten, proefschrift, Eindhoven (1979).

2. Het gebruik van de term "intermediaire fase" ter aanduiding van coëxistentiegebieden werkt verwarrend en dient derhalve vermeden te worden.

V.G. Bar'yakhtar, A.A. Galkin en V.T. Telepa,

Sov. Phys. Solid State 19, 1259 (1977).

I.M. Vitebskii en D.A. Yablonskii,

Sov. Phys. Solid State 19, 1978 (1977).

3. Bij de verifikatie van thermodynamische schalingshypotheseën in de omgeving van een (multi)kritiek punt speelt de zogenaamde "data collapsing" een belangrijke rol. Het is gewenst statistisch gefundeerde criteria voor de kwaliteit van deze "data collapsing" te ontwikkelen.

A.L.M. Bongaarts, W.J.M. de Jonge en P. van der Leeden,

Phys. Rev. Lett. 37, 1007 (1976).

N. Giordano en W.P. Wolf, AIP Conf. Proc. 29, 459 (1976).

E.K. Riedel, H. Meyer en R.P. Behringer,

J. Low Temp. Phys. 22, 369 (1976).

4. De precisie van warmtegeleidingsmetingen waarbij de temperatuur aan één zijde van het preparaat gestabiliseerd wordt geldt als veel groter dan die van methoden waarbij geen temperatuurstabilisatie wordt toegepast. Het wordt te weinig benadrukt (of beseft) dat de winst in nauwkeurigheid in het algemeen slechts behaald wordt in situaties waarin grote thermische overgangswaarden optreden.

H.N. de Lang, proefschrift, Nijmegen (1977).

M. Locatelli, Bull. Inf. Sc. Techn. 215, 39 (1976).

5. Bij de interpretatie van de susceptibiliteitsmetingen aan $\text{CsCoCl}_3 \cdot 2\text{H}_2\text{O}$ door McElearny wordt de zogeheten Van Vleck bijdrage ten onrechte verwaarloosd.

J.N. McElearny, Solid State Comm. 24, 863 (1977).

6. In mengkoelers kan de extra verdamping uit het ^4He -bad, die het gevolg is van de ^3He -cirkulatie, aanzienlijk gereduceerd worden door toepassing van warmtewisselaars tussen de inkomende en uitgaande ^3He -gasstromen boven 4.2 K.
7. Met het samenstellen van lesroosters voor het voortgezet onderwijs zijn momenteel in Nederland volgens een globale schatting 200 manjaar per jaar gemoeid. Ondersteuning van deze activiteit door middel van een centraal beheerd computerprogramma lijkt gewenst.
8. Indien het in de bedoeling van de overheid ligt door het invoeren van de Machtigingsregeling voor Algemene Radio Communicatie een mogelijkheid te scheppen tot het voeren van niet al te zeer gestoorde gesprekken tussen de verschillende gemachtigden, dan is de keuze van 22 kanalen in de 27 MHz band, gelet op de propagatie-eigenschappen van radiogolven met een dergelijke frequentie en het te verwachten aantal gemachtigden, aan ernstige bedenkingen onderhevig.

J.P.A.M. Hijmans

29 mei 1979.